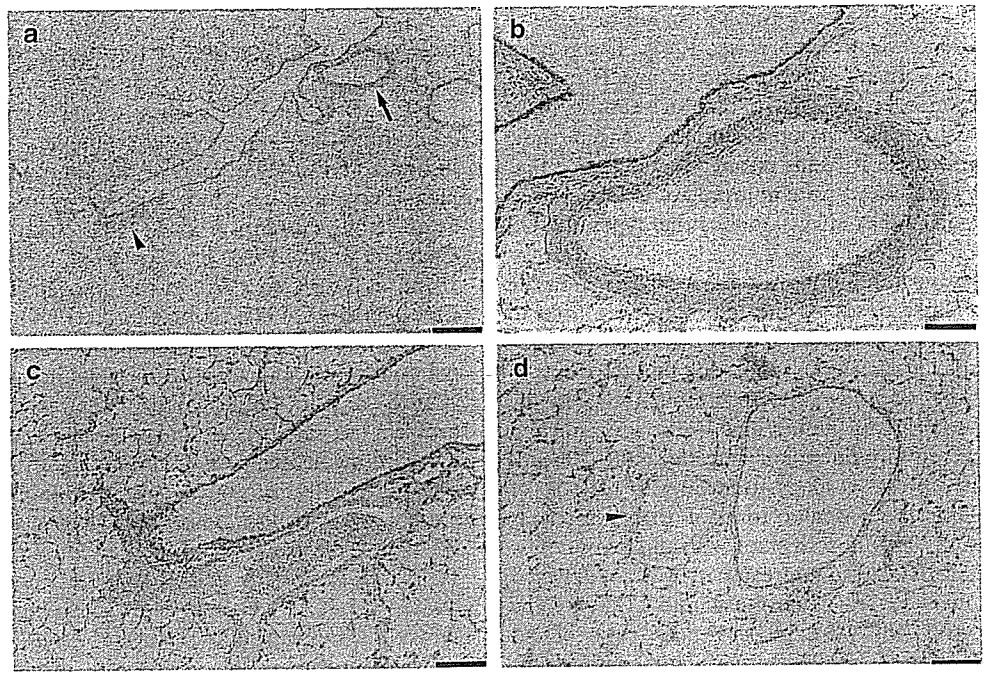

Figure 5 iNOS immunostaining of muscular pulmonary arteries of chronically hypoxic (a–c) and control (d) rats. (a) Low magnification view. iNOS-positive (arrow) and iNOS-negative (arrowhead) muscular pulmonary arteries are seen in the same section. (b, c) Higher magnification views of iNOS-positive and iNOS-negative arteries, respectively. (d) iNOS-negative muscular artery (arrowhead). Scale bars: (a) 500 μm, (b, c) 50 μm, (d) 100 μm.

Table 3 Pulmonary arteries positive and negative for NOS

	Elastic (400–700 μm)		*Muscular* (100–300 μm)		*Muscular* (<100 μm)	
	Positive	*Negative*	*Positive*	*Negative*	*Positive*	*Negative*
eNOS						
C	39 (90.7)	4 (9.3)	56 (50.9)	54 (49.1)	23 (8.9)	236 (91.1)
CH	43 (97.7)	1 (2.3)	97 (94.2)	6 (5.8)	210 (88.6)	27 (11.4)
iNOS						
C	4 (9.8)	37 (90.2)	7 (6.0)	109 (94.0)	4 (1.6)	252 (98.4)
CH	30 (68.2)	14 (31.8)	56 (55.4)	45 (44.6)	104 (43.7)	134 (56.3)

Values are presented as number (%). Number of NOS-positive and NOS-negative vessels was counted in control (C; $n=4$) and 4-week hypoxic (CH; $n=4$) rats.

sion to regulating tone at individual pulmonary arterial branches with natural blood circulation.

RV hypertrophy

The presence of pulmonary hypertension in rats breathing hypoxic air was reflected in an increased ratio of RV/LV + S, which averaged 0.62 ± 0.05 vs 0.33 ± 0.02 in normoxic controls. These ratios in the CH and control rats agree with those of others (Abraham *et al.*, 1971; Rabinovitch *et al.*, 1979; Muramatsu *et al.*, 1997).

ID constriction mechanisms in pulmonary arteries in response to NOS inhibitor injection

We showed that L-arginine injection completely abolishes the ID reductions in response to nonselective NOS inhibitors and iNOS selective NOS inhibitors in the pulmonary arteries. This suggests that inhibiting the basal release of NO derived from L-arginine is primarily responsible for the ID constrictions.

In the present study, L-NAME (50 mg kg^{-1} mg kg^{-1} i.v.) or L-NMMA (60 mg kg^{-1} i.v.) was used for nonselective NOS inhibition and L-canavanine (100 mg kg^{-1} i.v.) or *S*-methylisothiourea sulphate (3 mg kg^{-1} i.v.) for selective iNOS inhibition. We determined the doses of NOS inhibitors based on the previous data (Loeb & Longnecker, 1992; McCormack & Paterson, 1993; Oka *et al.*, 1993; Huang *et al.*, 1994; Szabo *et al.*, 1994; Teale & Atkinson, 1994; Liaudet *et al.*, 1996) and our preliminary dose–response data (see Methods). Previous studies (Teale & Atkinson, 1994; Liaudet *et al.*, 1996) have shown that L-canavanine (100 mg kg^{-1} i.v.) almost completely suppresses the lipopolysaccharide-induced hypotension in anaesthetized rats, although it does not significantly affect blood pressure in the absence of lipopolysaccharide. *S*-methylisothiourea sulphate (3 mg kg^{-1} i.v.) caused a potent pressor response in lipopolysaccharide-treated rats as com-

pared with control rats and a restoration of blood pressure to prelipopolysaccharide levels (Szabo *et al.*, 1994). The present study has shown a significant ID reduction in the CH rat, but no significant response in the control rat in response to L-canavanine and *S*-methylisothiourea sulphate. From these previous and present data, it seems reasonable to assume that the doses of iNOS inhibitors we employed were adequate to inhibit iNOS, but with minor effects on the other types of NOS *in vivo*.

For nNOS selective inhibition, we used 7-nitro indazole ($50\,mg\,kg^{-1}$ i.p.). These doses of the inhibitor were able to cause 60–80% reduction of nNOS activity in the rat (Kalisch *et al.*, 1996; Okamoto *et al.*, 1997), suggesting that the doses of nNOS inhibitor were also adequate to inhibit nNOS in the current study. Therefore, our finding that 7-nitro indazole had no significant effect on any pulmonary arteries (100–700 μm) of the control and CH rats is likely to mean that the role of nNOS in controlling the vascular tone of these vessels is minimal, if any at all. This is consistent with the immunohistochemical data that nNOS immunoreactivity was not detected in the small pulmonary vessels of normoxic and CH rats (Xue & Johns, 1996) and with the physiological data of no significant contribution of nNOS to modulating pulmonary vascular tone in the mouse (Fagan *et al.*, 1999b) and cat (Shirai *et al.*, 1999). Our result also suggests that sympathetic nerve activity increase caused by nNOS inhibition in the brain stem (Umans, 1995) contributed little to the nonselective NOS inhibitor-induced ID reduction.

The contribution of pressure- and flow-sensing mechanisms (Bevan & Laher, 1991) to the NOS inhibitor-induced ID response has been discussed. There was a PAP elevation of ~3 mmHg in response to nonselective NOS inhibitors in the CH rat (Table 2), suggesting the possibility that the pressure-sensing mechanism influenced the ID change pattern caused by the local action of nonselective NOS inhibitor on the small pulmonary arteries. To examine this possibility, we measured ID changes of the pulmonary vessels in response to mechanically induced increases in PAP. No significant ID change was found in response to ~4 mmHg PAP rise, suggesting that this possibility is small.

Pulmonary blood flow was not measured in this study, but it was reported that cardiac output decreases by 15–40% in response to nonselective NOS inhibitor in normoxic (Loeb & Longnecker, 1992; McCormack & Paterson, 1993; Oka *et al.*, 1993; Huang *et al.*, 1994) and chronically hypoxic rats (Oka *et al.*, 1993) and did not significantly change with iNOS selective inhibitors in these rats (Liaudet *et al.*, 1996; Resta *et al.*, 1999). Therefore, another possibility is that the flow-sensing mechanism affected the ID change pattern in response to nonselective NOS inhibitor administration. However, in preliminary experiments, we found no significant ID change in response to ~40% decrease in pulmonary blood flow caused by partially occluding the circumference of inferior vena cava with a 4-0 silk ligature. This suggested that this possibility is also small.

However, these results cannot completely exclude these possibilities, since we did not determine the local pressure- and flow-mediated vasomotor responses at different serial segments of the pulmonary vessels. To determine these responses, it would be necessary to measure directly the local pressure and flow velocity at the same site where vascular dimensions are being assessed.

Contribution of endogenous NO to controlling basal pulmonary vascular tone in normoxic rats

Previous pressure-flow studies have shown that nonselective NOS inhibitors increase basal pulmonary vascular resistance in intact and isolated lungs of the lamb, pig, rabbit, cat, and man (Persson *et al.*, 1990; Fineman *et al.*, 1991; McMahon *et al.*, 1991; Gordon & Tod, 1993; Nelin & Dawson, 1993; Cremona *et al.*, 1994; Stamler *et al.*, 1994; Albertini *et al.*, 1996), although no effect in the dog (Nishiwaki *et al.*, 1992; Cremona *et al.*, 1994; Leeman *et al.*, 1994). This suggests that endogenous NO plays a contributory role in regulating basal pulmonary vascular tone for all these animals except the dog (Barnes & Liu, 1995). On the other hand, in the rat, this problem has mainly been studied using isolated perfused lungs, but with inconsistent results. Many investigators have shown no or little effect of nonselective NOS inhibitors on the basal pulmonary vascular resistance (Robertson *et al.*, 1990; Hasunuma *et al.*, 1991; Barer *et al.*, 1993; Hampl *et al.*, 1993; McCormack & Paterson, 1993; Russ & Walker, 1993; Isaacson *et al.*, 1994; Resta *et al.*, 1999), although others have shown a significant effect (Barnard *et al.*, 1993; Roos *et al.*, 1996; Cadogan *et al.*, 1999). In the present study, we considered the change in ID to be better explained as an index of local vasomotor response in a given vessel than the change in calculated resistance estimated from the pressure–flow relation. Therefore, we directly measured ID changes of the rat pulmonary arteries using an X-ray TV system (Sada *et al.*, 1985; Shirai *et al.*, 1986). Our data showed that nonselective NOS inhibitor injection causes a significant ID reduction in both muscular (100–300 μm) and elastic (400–700 μm) segment levels in normoxic control rats (Figure 2). Relative frequency distribution of ID response showed that the peak of the frequency curve of the elastic arteries is located on the more constrictor side than that of the muscular arteries, and that the constrictor response occurs in most of the elastic arteries but only in about half of the muscular arteries (Figure 3). This suggests greater effects of NO on basal tone of the elastic pulmonary arteries and lesser effects for the muscular arteries in the normoxic rat. Moreover, there was the coexistence of relatively small magnitudes of constrictions and no change with similar frequencies among parallel-arranged muscular arteries (Figure 3). This ID response pattern may partly explain the previous data of no or little change in the pressure–flow relation of the entire lung (Robertson *et al.*, 1990; Hasunuma *et al.*, 1991; Barer *et al.*, 1993; Hampl *et al.*, 1993; McCormack & Paterson, 1993; Russ & Walker, 1993; Isaacson *et al.*, 1994; Resta *et al.*, 1999) and the present data of no significant PAP rise in response to nonselective NOS inhibition, if we assume that local redistributions of blood flow from constricted to nonconstricted muscular arteries occurred and then recruited new peripheral channels such as capillaries, maintaining entire pulmonary vascular resistance within nearly baseline levels. In addition, because the previous pressure–flow studies were mostly performed in constant perfused lungs, a decrease in NO production due to the artificial perfusate composition (Sprague *et al.*, 1995) and/or mechanical flow pattern (Hakim, 1994) may have occurred in these studies, making it more difficult to detect the small magnitude of vasoconstriction due to NOS inhibition in the muscular arteries.

The present study also demonstrated that selective inhibitors of iNOS had no significant effects on any levels of the arteries observed in control rats (Figure 2). Relative frequency distribution of ID response showed that iNOS selective inhibition causes no ID changes in ~80% of the muscular and elastic arteries, and small magnitudes of ID constriction in the remaining arteries (Figure 3). The data suggest a minor contribution of iNOS-derived NO to basal tone regulation in both muscular and elastic arteries, and probably explain the findings that selective iNOS inhibition had no effect on the baseline pulmonary vascular resistance in the rat (Resta *et al.*, 1999). Moreover, considering in connection with the above-mentioned suggestion of minor role of nNOS in regulating vascular tone of the muscular and elastic arteries, the present study suggests that, during normoxia, the predominant isoform of NOS regulating basal tone of these arteries is eNOS. This is consistent with the findings in the mouse that baseline pulmonary arterial pressure in eNOS null lungs significantly increased compared with wild type (Steudel *et al.*, 1997; Fagan *et al.*, 1999b), but the pressure in iNOS null lungs and nNOS null lungs did not (Fagan *et al.*, 1999b). We have also suggested the primary role of eNOS in regulating basal ID of the 100–1700 μm cat pulmonary arteries including muscular and elastic segments (Shirai *et al.*, 1999).

The present immunohistochemical analyses in the control rat have shown that eNOS-positive vessels were found in 91% of the elastic arteries >400 μm, but only in 9–51% of muscular arteries <300 μm (Table 3). This is consistent with the previous rat data that eNOS immunoreactivity is distributed among 96% of the pulmonary vessels (>150 μm ID), but only in 2–20% of the vessels smaller than this (Xue & Johns, 1996). The iNOS distribution data (Table 3) also agree with the previous data of very limited iNOS expression in vascular smooth muscle of all normoxic rat pulmonary arteries (Xue *et al.*, 1994; Xue & Johns, 1996; Cadogan *et al.*, 1999). We have further shown that in normoxic lungs, such eNOS and iNOS immunoreactivity distributions are almost in accord with the frequency distributions of ID constriction due to nonselective and iNOS selective inhibition, respectively (Figure 3).

Regional differences in vasodilator effect of endogenous NO in chronically hypoxic pulmonary arteries

It is generally agreed that main and extralobar pulmonary arteries isolated from CH rats have blunted endothelium-dependent relaxation to various receptor-dependent vasodilators (Crawley *et al.*, 1992; Rodman, 1992; Carville *et al.*, 1993; Shaul *et al.*, 1993; Maruyama & Maruyama, 1994) and to receptor-independent Ca^{2+} ionophore A-23187 (Carville *et al.*, 1993; Shaul *et al.*, 1993). However, different results have been obtained concerning whether CH alters the NO-mediated basal tone regulation in these proximal elastic pulmonary arteries. Some researchers have suggested that the effect of nonselective NOS inhibitor on basal tone is not significantly changed by CH (Rodman, 1992; Maruyama & Maruyama, 1994), whereas others have suggested its enhancement (Oka *et al.*, 1993). Moreover, basal NO production assessed by measuring cyclic guanosine-3′,5′-monophosphate (GMP) synthesis has been shown to decrease in main pulmonary arteries during chronic hypoxia (Shaul *et al.*, 1993). The present study showed that, in the transitional elastic arteries (400–500 μm), the nonselective NOS inhibitor-induced ID reduction is slightly but significantly larger in the CH rat than in the control rat, although no significant difference is present in the classical elastic arteries (600–700 μm) (Figure 2). In addition, the frequency distribution of ID response showed that the CH distribution curve is located slightly on the more constrictor side than the control curve in the transitional arteries, whereas no clear difference exists between these curves in the classical arteries (Figure 3). These results suggest that within the intralobar elastic arteries, small but significant degree of an enhancement of the NO-mediated basal vascular tone regulation is caused locally in the most distal vascular segment.

In the muscular pulmonary arteries (100–300 μm ID), there has been no direct observation on the change in NO-mediated control of basal vascular tone in response to CH. The present study has for the first time supplied information on the muscular arteries that the ID reduction due to nonselective NOS inhibition is significantly larger in the CH rat than in the control rat (Figure 2). Frequency distribution of ID response due to nonselective NOS inhibition showed that the CH distribution curve is located extremely on the more constrictor side than the control curve. Moreover, significant constriction was almost all ID responses in the CH vessels, but about half in the control vessels (Figure 3). These ID response patterns suggest that an increase in NO-mediated suppression of basal vascular tone occurs in most branches of the muscular arteries during CH, and probably explain the previous findings (Barer *et al.*, 1993; Oka *et al.*, 1993; Isaacson *et al.*, 1994; Roos *et al.*, 1996) that nonselective NOS inhibitor increased calculated resistance more greatly in perfused lungs obtained from CH rats than in those from normoxic rats.

It has recently been shown that iNOS inhibition with L-N^6-(1-iminoethyl)lysine dihydrochloride does not alter the dose–response change in calculated pulmonary arterial and venous resistance due to U-46619 in isolated, saline-perfused lungs from CH rats (Resta *et al.*, 1999). Moreover, this inhibition had no significant effect on PAP, SAP, and cardiac output in conscious hypoxic rats. From these data, they concluded that NO derived from iNOS does not modulate pulmonary vasoconstrictor responsiveness during CH (Resta *et al.*, 1999). The present study similarly showed that during iNOS inhibition (with L-canavanine or *S*-methylisothiourea), PAP and SAP did not significantly change in the CH rat (Table 2). However, we simultaneously found that there were significant ID reductions mainly in the muscular pulmonary arteries (Figure 2). Moreover, the frequency distribution of the ID response during iNOS inhibition showed that the CH distribution curve is located on the more constrictor side than the control curve in the muscular arteries, but, about half of the CH muscular arteries still exhibited no change, in contrast to the case of nonselective NOS inhibition (Figure 3). Therefore, for the same possible reason (local redistributions of flow from constricted to nonconstricted arteries) as mentioned above in the heterogenous vasoconstrictor effect of nonselective NOS inhibition on normoxic rats, we suppose that such a coexistence of ID constriction and no change in the parallel-arranged arteries during iNOS inhibition is also difficult to detect from changes in the pulmonary pressure–flow relation.

Previous studies have shown that in 2–4-week hypoxic rats, NOS immunoreactivity became markedly positive in the endothelial cells of most 80–150 μm pulmonary arteries

compared with normoxic rats (Xue *et al.*, 1994) and that the percentages (~95%) of eNOS-positive pulmonary vessels >150 μm ID are similar in 0–7-day hypoxic rats (Xue & Johns, 1996). Our findings that the percentages of eNOS-positive muscular arteries greatly rose up to 89–94% in the 4-week hypoxic lung, but those for elastic arteries displayed a slight increase (Table 3), support the previous data. However, we also provided new information that the eNOS distribution change corresponds well to the hypoxic change in the distribution of nonselective NOS inhibitor-induced ID reduction (Figure 3). On the other hand, iNOS protein has been shown to increase in the vascular smooth muscle of both muscular and elastic arteries obtained from CH rats (Xue *et al.*, 1994; Xue & Johns, 1996). For the first time, we found that 4-week hypoxia increases iNOS immunoreactivity scatteringly among the muscular and elastic arteries (Figure 5 and Table 3). The iNOS distribution in the muscular arteries was in accord with the distribution of iNOS inhibitor-induced ID reduction in these arteries (Figure 3). However, the increase in iNOS expression in the elastic arteries seems to be inconsistent with the data showing no significant effect of iNOS selective inhibition and no enhancement of nonselective NOS inhibitor effect in these arteries (Figures 2 and 3). The reason for this discrepancy remains to be elucidated. However, it has been shown that CH increases cyclic GMP phosphodiesterase activity in the larger intrapulmonary elastic arteries in the rat, but does not change it in the muscular arteries (MacLean *et al.*, 1997). It is therefore possible that in the elastic arteries, increased production of NO from iNOS cannot rise cyclic GMP level due to an increase in activity of cyclic GMP phosphodiesterase enzymes which catalyse cyclic GMP hydrolysis, while it can increase cyclic GMP level in the muscular arteries.

Together with the present finding of no significant ID response to nNOS inhibition, we conclude that in CH rats, both vasodilator effects of eNOS- and iNOS-derived NO are enhanced primarily in the muscular pulmonary arteries (100–300 μm); the enhancement of eNOS effects is induced extensively in these arteries, while that for iNOS sporadically in them. This is consistent with the previous data (Steudel *et al.*, 1998; Fagan *et al.*, 1999a, b) of marked pulmonary hypertension in eNOS-deficient mice raised in chronic hypoxia when compared with wild type, and suggests that NO production by eNOS is vital to counterbalance hypoxic pulmonary vasoconstriction, which is localized in muscular arteries (Shirai *et al.*, 1986; 1997; Barnes & Liu, 1995; Weir & Archer, 1995) and serves to inhibit the progress of pulmonary hypertension.

Possible factors responsible for nonuniform iNOS increase in hypoxic pulmonary arteries

iNOS was expressed in about half of the muscular pulmonary arteries of the chronic hypoxic rat, while eNOS in almost all these vessels (Table 3). It has been suggested that in the rat, the increase in eNOS expression after chronic hypoxia is due to the direct effect of hypoxia or hypoxia-induced factors independently of changes in haemodynamics (Everett *et al.*, 1998; Le Cras *et al.*, 1998). Therefore, it is possible that during chronic hypoxia, almost all muscular pulmonary arteries were exposed to low oxygen tension and, in turn, the upregulation of eNOS was induced in these arteries. On the other hand, the increase in iNOS expression may be caused by flow/wall shear stress (Rairigh *et al.*, 1999; Gosgnach *et al.*, 2000). We have previously shown that during acute inhalation of 5% O_2, ~60% of branches constrict in 100–200 μm feline muscular pulmonary arteries, but others display no significant response (Shirai *et al.*, 1986), meaning that hypoxia does not result in uniformly distributed pulmonary vasoconstriction. Acute hypoxia has also been shown to increase the heterogeneity of pulmonary vascular transit times throughout dog lung lobe (Dawson *et al.*, 1983). Moreover, chronic hypoxia at high altitude has been suggested to induce inhomogenous pulmonary vasoconstriction and regional overperfusion (Richalet, 1995; Hultgren, 1996; Bartsch, 1997). Such heterogenous distribution of vasoconstriction and blood flow may regionally increase shear stress and damage vascular endothelium (Richalet, 1995; West *et al.*, 1995; Bartsch, 1997; Botney, 1999). Indeed, endothelial injury with swelling in small peripheral arteries was observed in chronically hypoxic rats (Meyrick & Reid, 1978). Thus, we suggest a possibility that the heterogenous shear force distribution induced the vascular smooth muscle iNOS expression sporadically among the muscular pulmonary arteries (Figure 5 and Table 3) through the release of inflammatory mediators such as cytokines and eicosanoids and adhesion molecules (Richalet, 1995; Bartsch, 1997; Schoene *et al.*, 1988; Hansson *et al.*, 1994; Kubo *et al.*, 1996; Rabinovitch, 1997) and/or oxidative stress-induced NF-κ B activation after endothelial damage (Gosgnach *et al.*, 2000).

In conclusion, we suggest that, in 4-week hypoxia rats, functional and histological upregulation of eNOS and iNOS occurs chiefly in the muscular segments of pulmonary arteries. The eNOS upregulation is induced extensively in the muscular arteries, but the iNOS upregulation sporadically among these arteries. nNOS has no significant vasodilator effect. Such eNOS and iNOS upregulation may contribute to attenuating hypoxic pulmonary vasoconstriction which is localized in the muscular segments and, in turn, inhibit the progress of pulmonary hypertension.

This study was supported, in part, by a grant for the 'Ground Research for Space Utilization' promoted by NASDA and the Japan Space Forum; by Grants-in-Aid for Scientific Research from the Ministry of Education, Culture, Sports, Science, and Technology; by the Promotion of Fundamental studies in Health Science of the Organization for Pharmacological Safety and Research (OPSR); and by Health Sciences Grants (Funds for Human Genome Research and Regeneration Medicine Research, Japan.

References

ABRAHAM, A.S., KAY, J.M., COLE, R.B. & PINCOCK, A.C. (1971). Haemodynamic and pathological study of the effect of chronic hypoxia and subsequent recovery of the heart and pulmonary vasculature of the rat. *Cardiovasc. Res.*, **5**, 95–102.

ADNOT, S., RAFFESTIN, B., EDDAHIBI, S., BRAQUET, P. & CHABRIER, P.-E. (1991). Loss of endothelium-dependent relaxant activity in the pulmonary circulation of rats exposed to chronic hypoxia. *J. Clin. Invest.*, **87**, 155–162.

ALBERTINI, M., VANELLI, G. & CLEMENT, G. (1996). PGI_2 and nitric oxide involvement in the regulation of systemic and pulmonary basal vascular tone in the pig. *Prostaglandins Leukotr. Essent. Fatty Acids*, **54**, 273–278.

BARER, G., EMERY, C., STEWART, A., BEE, D. & HOWARD, P. (1993). Endothelial control of the pulmonary circulation in normal and chronically hypoxic rats. *J. Physiol.*, **463**, 1–16.

BARNARD, J.W., WILSON, P.S., MOORE, T.M., THOMPSON, W.J. & TAYLOR, A.E. (1993). Effect of nitric oxide and cyclooxygenase products on vascular resistance in dog and rat lungs. *J. Appl. Physiol.*, **74**, 2940–2948.

BARNES, P.J. & LIU, S.F. (1995). Regulation of pulmonary vascular tone. *Pharmacol. Rev.*, **47**, 87–131.

BARTSCH, P. (1997). High altitude pulmonary edema. *Respiration*, **64**, 435–443.

BEVAN, J.A. & LAHER, I. (1991). Pressure and flow-dependent vascular tone. *FASEB J.*, **5**, 2267–2273.

BOTNEY, M.D. (1999). Role of hemodynamics in pulmonary vascular remodeling. *Am. J. Respir. Crit. Care Med.*, **159**, 361–364.

CADOGAN, E., HOPKINS, N., GILES, S., BANNIGAN, J.G., MOYNIHAN, J. & MCLOUGHLIN, P. (1999). Enhanced expression of inducible nitric oxide synthase without vasodilator effect in chronically infected lungs. *Am. J. Physiol.*, **277**, L616–L627.

CARVILLE, C., RAFFESTIN, B., EDDAHIBI, S., BLOUQUIT, Y. & ADNOT, S. (1993). Loss of endothelium-dependent relaxation in proximal pulmonary arteries from rats exposed to chronic hypoxia: effects of *in vivo* and *in vitro* supplementation with L-arginine. *J. Cardiovasc. Pharmacol.*, **22**, 889–896.

CRAWLEY, D.E., ZHAO, L., GIEMBYCZ, M.A. & LIU, S. (1992). Chronic hypoxia impairs soluble guanylyl cyclase-mediated pulmonary arterial relaxation in the rat. *Am. J. Physiol.*, **263**, L325–L332.

CREMONA, G., WOOD, A.M., HALL, L.W., BOWER, E.A. & HIGENBOTTAM, T. (1994). Effect of inhibitors of nitric oxide release and action on vascular tone in isolated lungs of pig, sheep, dog and man. *J. Physiol.*, **481**, 185–195.

DAWSON, C.A., BRONIKOWSKI, T.A., LINEHAN, J.H. & HAKIM, T.S. (1983). Influence of pulmonary vasoconstriction on ling water and perfusion heterogeneity. *J. Appl. Physiol.*, **54**, 654–660.

EDDAHIBI, S., ADNOT, S., CARVILLE, C., BLOUQUIT, Y. & RAFFESTIN, B. (1992). L-Arginine restores endothelium-dependent relaxation in pulmonary circulation of chronically hypoxic rats. *Am. J. Physiol.*, **263**, L194–L200.

EVERETT, A.D., LE CRAS, T.D., XUE, C. & JOHNS, R.A. (1998). eNOS expression is not altered in pulmonary vascular remodeling due to increased pulmonary blood flow. *Am. J. Physiol.*, **274**, L1058–L1065.

FAGAN, K.A., FOUTY, B.W., TYLER, R.C., MORRIS JR, K.G., HEPLER, L.K., SATO, K., LE CRAS, T.D., ABMAN, S.H., WEINBERGER, H.D., HUANG, P.L., MCMURTRY, I.F. & RODMAN, D.M. (1999a). The pulmonary circulation of homozygous or heterozygous eNOS-null mice is hyperresponsive to mild hypoxia. *J. Clin. Invest.*, **103**, 291–299.

FAGAN, K.A., TYLER, R.C., SATO, K, FOUTY, B.W., Morris JR, K.G., HUANG, P.L., MCMURTRY, I.F. & RODMAN, D.M. (1999b). Relative contributions of endothelial, inducible, and neuronal NOS to tone in the murine pulmonary circulation. *Am. J. Physiol.*, **277**, L472–L478.

FINEMAN, J.R., HEYMANN, M.A. & SOIFER, S.J. (1991). N^{ω}-nitro-L-arginine attenuates endothelium-dependent pulmonary vasodilation in lambs. *Am. J. Physiol.*, **260**, H1299–H1306.

GORDON, J.B. & TOD, M.L. (1993). Effects of N^{ω}-nitro-L-arginine on total and segmental vascular resistances in developing lamb lungs. *J. Appl. Physiol.*, **75**, 76–85.

GOSGNACH, W., MESSIKA-ZEITOUN, D., GONZALEZ, W., PHILIPE, M. & MICHEL, J.-B. (2000). Shear stress induces iNOS expression in cultured smooth muscle cells: roles of oxidative stress. *Am. J. Physiol.*, **279**, C1880–C1888.

HAKIM, T.S. (1994). Flow-induced release of EDRF in the pulmonary vasculature: site of release and action. *Am. J. Physiol.*, **267**, H363–H369.

HAMPL, V., ARCHER, S.L., NELSON, D.P. & WEIR, E.K. (1993). Chronic EDRF inhibition and hypoxia: effects on pulmonary circulation and systemic blood pressure. *J. Appl. Physiol.*, **75**, 1748–1757.

HANSSON, G.K., GENG, Y.-J., HOLM, J., HARDHAMMAR, P., WENNMALM, A. & JENNISCHE, E. (1994). Arterial smooth muscle cells express nitric oxide synthase in response to endothelial injury. *J. Exp. Med.*, **180**, 733–738.

HASUNUMA, K., YAMAGUCHI, T., RODMAN, D.M., O'BRIEN, R.F. & MCMURTRY, I.F. (1991). Effects of inhibitors of EDRF and EDHF on vasoreactivity of perfused rat lungs. *Am. J. Physiol.*, **260**, L97–L104.

HUANG, M., LEBLANC, M.L. & HESTER, R.L. (1994). Systemic and regional hemodynamics after nitric oxide synthase inhibition: role of a neurogenic mechanism. *Am. J. Physiol.*, **267**, R84–R88.

HULTGREN, H.N. (1996). High-altitude pulmonary edema: current concepts. *Annu. Rev. Med.*, **47**, 267–284.

ISAACSON, T.C., HAMPL, V., WEIR, E.K., NELSON, D.P. & ARCHER, S.L. (1994). Increased endothelium-derived NO in hypertensive pulmonary circulation of chronically hypoxic rats. *J. Appl. Physiol.*, **76**, 933–940.

KALISCH, B.E., CONNOP, B.P., JHAMANDAS, K., BENINGER, R.J. & BOEGMAN, R.J. (1996). Differential action of 7-nitro indazole on rat brain nitric oxide synthase. *Neurosci. Lett.*, **219**, 75–78.

KAY, J.M. (1983). Pulmonary vasculature and nerves. Comparative morphologic features of the pulmonary vasculature in mammals. *Am. Rev. Respir. Dis.*, **128**, S53–S57.

KUBO, K, HANAOKA, M., YAMAGUCHI, S., HAYANO, T., HAYASAKA, M., KOIZUMI, T., FUJIMOTO, K., KOBAYASHI, T. & HONDA, T. (1996). Cytokines in bronchoalveolar lavage fluid in patients with high altitude pulmonary oedema at moderate altitude in Japan. *Thorax*, **51**, 739–742.

LE CRAS, T.D., TYLER, R.C., HORAN, M.P., MORRIS, K.G., TUDER, R.M. & MCMURTRY, I.F. (1998). Effects of chronic hypoxia and altered hemodynamics on endothelial nitric oxide synthase expression in the adult rat lung. *J. Clin. Invest.*, **101**, 795–801.

LE CRAS, T.D., XUE, C., RENGASAMY, A. & JOHNS, R.A. (1996). Chronic hypoxia upregulates endothelial and inducible NO synthase gene and protein expression in rat lung. *Am. J. Physiol.*, **270**, L164–L170.

LEEMAN, M., ZEGERS DE BEYL, V., DELCROIX, M. & NAEIJE, R. (1994). Effects of endogenous nitric oxide on pulmonary vascular tone in intact dogs. *Am. J. Physiol.*, **266**, H2343–H2347.

LIAUDET, L., FEIHL, F., ROSSELET, A., MARKERT, M., HURNI, J.-M. & PERRET, C. (1996). Beneficial effects of L-canavanine, a selective inhibitor of inducible nitric oxide synthase, during rodent endotoxaemia. *Clin. Sci.*, **90**, 369–377.

LOEB, A.L. & LONGNECKER, D.E. (1992). Inhibition of endothelium-derived relaxing factor-dependent circulatory control in intact rats. *Am. J. Physiol.*, **262**, H1494–H1500.

MACLEAN, M.R., JOHNSTON, E.D., MCCULLOCH, K.M., POOLEY, L., HOUSLAY, M.D. & SWEENEY, G. (1997). Phosphodiesterase isoforms in the pulmonary arterial circulation of the rat: changes in pulmonary hypertension. *J. Pharmacol. Exp. Ther.*, **283**, 619–624.

MARUYAMA, J. & MARUYAMA, K. (1994). Impaired nitric oxide-dependent responses and their recovery in hypertensive pulmonary arteries of rats. *Am. J. Physiol.*, **266**, H2476–H2488.

MCCORMACK, D.G. & PATERSON, N.A.M. (1993). Loss of hypoxic pulmonary vasoconstriction in chronic pneumonia is not mediated by nitric oxide. *Am. J. Physiol.*, **265**, H1523–H1528.

MCMAHON, T.J., HOOD, J.S., BELLAN, J.A. & KADOWITZ, P.J. (1991). N^{ω}-nitro-L-arginine methyl ester selectively inhibits pulmonary vasodilator responses to acetylcholine and bradykinin. *J. Appl. Physiol.*, **71**, 2026–2031.

MEYRICK, B. & REID, L. (1978). The effect of continued hypoxia on rat pulmonary arterial circulation. An ultrastructural study. *Lab. Invest.*, **38**, 188–200.

MOORE, P.K., WALLACE, P., GAFFEN, Z., HART, S.L. & BABBEDGE, R.C. (1993). Characterization of the novel nitric oxide synthase inhibitor 7-nitro indazole and related indazoles: antinociceptive and cardiovascular effects. *Br. J. Pharmacol.*, **110**, 219–224.

MURAMATSU, M., RODMAN, D.M., OKA, M. & MCMURTRY, I.F. (1996). Thapsigargin stimulates NO activity in hypoxic hypertensive rat lungs and pulmonary arteries. *J. Appl. Physiol.*, **80**, 1336–1344.

MURAMATSU, M., RODMAN, D.M., OKA, M. & MCMURTRY, I.F. (1997). Endothelin-1 mediates nitro-L-arginine vasoconstriction of hypertensive rat lungs. *Am. J. Physiol.*, **272**, L807–L812.

NELIN, L.D. & DAWSON, C.A. (1993). The effect of N^{ω}-nitro-L-arginine methyl ester on hypoxic vasoconstriction in the neonatal pig lung. *Pediatr. Res.*, **34**, 349–353.

NISHIWAKI, K., NYHAN, D.P., ROCK, P., DESAI, P.M., PETERSON, W.P., PRIBBLE, C.G. & MURRAY, A. (1992). N^{ω}-nitro-L-arginine and pulmonary vascular pressure–flow relationship in conscious dogs. *Am. J. Physiol.*, **262**, H1331–H1337.

OKA, M., HASUNUMA, K., WEBB, S.A., STELZNER, T.J., RODMAN, D.M. & MCMURTRY, I.F. (1993). EDRF suppresses an unidentified vasoconstrictor mechanism in hypertensive rat lungs. *Am. J. Physiol.*, **264**, L587–L597.

OKAMOTO, H., HUDETZ, A.G., ROMAN, R.J., BOSNJAK, Z.J. & KAMPINE, J.P. (1997). Neuronal NOS-derived NO plays permissive role in cerebral blood flow response to hypercapnia. *Am. J. Physiol.*, **272**, H559–H566.

PERSSON, M.G., GUSTAFSSON, L.E., WIKLUND, N.P., MONCADA, S. & HEDQVIST, P. (1990). Endogenous nitric oxide as a probable modulator of pulmonary circulation and hypoxic pressor response *in vivo*. *Acta Physiol. Scand.*, **140**, 449–457.

RABINOVITCH, M. (1997). Pulmonary hypertension: updating a mysterious disease. *Cardiovasc. Res.*, **34**, 268–272.

RABINOVITCH, M., GAMBLE, W., NADAS, A.S., MIETTINEN, O.S. & REID, L. (1979). Rat pulmonary circulation after chronic hypoxia: hemodynamic and structural features. *Am. J. Physiol.*, **236**, H818–H827.

RAIRIGH, R.L., STORME, L., PARKER, T.A., LE CRAS, T.D., KINSELLA, J.P., JAKKULA, M. & ABMAN, S.H. (1999). Inducible NO synthase inhibition attenuates shear stress-induced pulmonary vasodilation in the ovine fetus. *Am. J. Physiol.*, **276**, L513–L521.

RESTA, T.C., GONZALES, R.J., DAIL, W.G., SANDERS, T.C. & WALKER, B.R. (1997). Selective upregulation of arterial endothelial nitric oxide synthase in pulmonary hypertension. *Am. J. Physiol.*, **272**, H806–H813.

RESTA, T.C., O'DONAUGHY, T.L., EARLEY, S., CHICOINE, L.G. & WALKER, B.R. (1999). Unaltered vasoconstrictor responsiveness after iNOS inhibition in lungs from chronically hypoxic rats. *Am. J. Physiol.*, **276**, L122–L130.

RESTA, T.C. & WALKER, B.R. (1996). Chronic hypoxia selectively augments endothelium-dependent pulmonary arterial vasodilation. *Am. J. Physiol.*, **270**, H888–H896.

RICHALET, J.-P. (1995). High altitude pulmonary oedema: still a place for controversy? *Thorax*, **50**, 923–929.

ROBERTSON, B.E., WARREN, J.B. & NYE, P.C.G. (1990). Inhibition of nitric oxide synthesis potentiates hypoxic vasoconstriction in isolated rat lungs. *Exp. Physiol.*, **75**, 255–257.

RODMAN, D.M. (1992). Chronic hypoxia selectively augments rat pulmonary artery Ca^{2+} and K^{+} channel-mediated relaxation. *Am. J. Physiol.*, **263**, L88–L94.

ROOS, C.M., FRANK, D.U., XUE, C., JOHNS, R.A. & RICH, G.F. (1996). Chronic inhaled nitric oxide: effects on pulmonary vascular endothelial function and pathology in rats. *J. Appl. Physiol.*, **80**, 252–260.

RUSS, R.D. & WALKER, B.R. (1993). Maintained endothelium-dependent pulmonary vasodilation following chronic hypoxia in the rat. *J. Appl. Physiol.*, **74**, 339–344.

SADA, K., SHIRAI, M. & NINOMIYA, I. (1985). X-ray TV system for measuring microcirculation in small pulmonary vessels. *J. Appl. Physiol.*, **59**, 1013–1018.

SASAKI, S.-I., KOBAYASHI, N., DAMBARA, T., KIRA, S. & SAKAI, T. (1995). Structural organization of pulmonary arteries in the rat lung. *Anat. Embryol.*, **191**, 477–489.

SCHOENE, R.B., SWENSON, E.R., PIZZO, C.J., HACKETT, P.H., ROACH, R.C., MILLS JR, W.J., HENDERSON JR, W.R. & MARTIN, T.R. (1988). The lung at high altitude: bronchoalveolar lavage in acute mountain sickness and pulmonary edema. *J. Appl. Physiol.*, **64**, 2605–2613.

SHAUL, P.W., NORTH, A.J., BRANNON, T.S., UJIIE, K., WELLS, L.B., NISEN, P.A., LOWENSTEIN, C.J., SNYDER, S.H. & STAR, R.A. (1995). Prolonged *in vivo* hypoxia enhances nitric oxide synthase type I and type III gene expression in adult rat lung. *Am. J. Respir. Cell Mol. Biol.*, **13**, 167–174.

SHAUL, P.W., WELLS, L.B. & HORNING, K.M. (1993). Acute and prolonged hypoxia attenuates endothelial nitric oxide production in rats pulmonary arteries by different mechanisms. *J. Cardiovasc. Pharmacol.*, **22**, 819–827.

SHIRAI, M., IKEDA, S., MIN, K.-Y., SHIMOUCHI, A., KAWAGUCHI, A.T. & NINOMIYA, I. (1999). Segmental differences in vasodilatation due to basal NO release in *in vivo* cat pulmonary vessels. *Respir. Physiol.*, **116**, 159–169.

SHIRAI, M., SADA, K. & NINOMIYA, I. (1986). Effects of regional alveolar hypoxia and hypercapnia on small pulmonary vessels in cats. *J. Appl. Physiol.*, **61**, 440–448.

SHIRAI, M., SHIMOUCHI, A., KAWAGUCHI, A.T., IKEDA, S., SUNAGAWA, K. & NINOMIYA, I. (1997). Endogenous nitric oxide attenuates hypoxic pulmonary vasoconstriction of small pulmonary arteries and veins in anaesthetized cats. *Acta Physiol. Scand.*, **159**, 263–264.

SPRAGUE, R.S., STEPHENSON, A.H., DIMMITT, R.A., WEINTRAUB, N.A., BRANCH, L., MCMURDO, L. & LONIGRO, A.J. (1995). Effect of L-NAME on pressure–flow relationships in isolated rabbit lungs: role of red blood cells. *Am. J. Physiol.*, **269**, H1941–H1948.

STAMLER, J.S., LOH, E., RODDY, M.-A., CURRIE, K.E. & CREAGER, M.A. (1994). Nitric oxide regulates basal systemic and pulmonary vascular resistance in healthy humans. *Circulation*, **89**, 2035–2040.

STEUDEL, W., ICHINOSE, F., HUANG, P.L., HURFORD, W.E., JONES, R.C., BEVAN, J.A., FISHMAN, M.C. & ZAPOL, W.M. (1997). Pulmonary vasoconstriction and hypertension in mice with targeted disruption of the endothelial nitric oxide synthase (NOS 3) gene. *Circ. Res.*, **81**, 34–41.

STEUDEL, W., SCHERRER-CROSBIE, M., BLOCH, K.D., WEIMANN, J., HUANG, P.L., JONES, R.C., PICARD, M.H. & ZAPOL, W.M. (1998). Sustained pulmonary hypertension and right ventricular hypertrophy after chronic hypoxia in mice with congenital deficiency of nitric oxide synthase 3. *J. Clin. Invest.*, **101**, 2468–2477.

SZABO, C., SOUTHAN, G.J. & THIEMERMANN, C. (1994). Beneficial effects and improved survival in rodent models of septic shock with *S*-methylisothiourea sulfate, a potent and selective inhibitor of inducible nitric oxide synthase. *Proc. Natl. Acad. Sci. U.S.A.*, **91**, 12472–12476.

TEALE, D.M. & ATKINSON, A.M. (1994). L-Canavanine restores blood pressure in a rat model of endotoxin shock. *Eur. J. Pharmacol.*, **271**, 87–92.

TYLER, R.C., MURAMATSU, M., ABMAN, S.H., STELZNER, T.J., RODMAN, D.M., BLOCH, K.D. & MCMURTRY, I.F. (1999). Variable expression of endothelial NO synthase in three forms of rat pulmonary hypertension. *Am. J. Physiol.*, **276**, L297–L303.

UMANS, J.G. (1995). Nitric oxide in the regulation of blood flow and arterial pressure. *Annu. Rev. Physiol.*, **57**, 771–790.

WEIR, E.K. & ARCHER, S. (1995). The mechanism of acute hypoxic pulmonary vasoconstriction: the tale of two channels. *FASEB J.*, **9**, 183–189.

WEST, J.B., COLICE, G.L., LEE, Y.-J., NAMBA, Y., KURDAK, S.S., FU, Z., OU, L.C. & MATHIEU-COSTELLO, O. (1995). Pathogenesis of high-altitude pulmonary oedema: direct evidence of stress failure of pulmonary capillaries. *Eur. Respir. J.*, **8**, 523–529.

XUE, C. & JOHNS, R.A. (1996). Upregulation of nitric oxide synthase correlates temporally with onset of pulmonary vascular remodeling in the hypoxic rat. *Hypertension*, **28**, 743–753.

XUE, C., RENGASAMY, A., LE CRAS, T.D., KOBERNA, P.A., DAILEY, G.C. & JOHNS, R.A. (1994). Distribution of NOS in normoxic vs hypoxic rat lung: upregulation of NOS by chronic hypoxia. *Am. J. Physiol.*, **267**, L667–L678.

(Received December 2, 2002
Revised March 3, 2003
Accepted April 7, 2003)

Evidence for Involvement of the Putative First Extracellular Loop in Differential Volume Sensitivity of the Na^+/H^+ Exchangers NHE1 and NHE2†

Xiaohua Su, Tianxiang Pang, Shigeo Wakabayashi,* and Munekazu Shigekawa

Department of Molecular Physiology, National Cardiovascular Center Research Institute, Fujishirodai 5-7-1, Suita, Osaka 565-8565, Japan

Received June 20, 2002; Revised Manuscript Received December 2, 2002

ABSTRACT: We studied hyperosmolarity-induced changes in cell volume and cytoplasmic pH in PS120 cells expressing Na^+/H^+ exchanger (NHE) isoforms and their mutants. Change in cell volume was estimated by measuring change in cell height by means of confocal microscopy. Regulatory volume increase (RVI) and cytoplasmic alkalinization were observed in cells expressing NHE1 but not in cells expressing NHE2 or NHE3. Studies using chimeric exchangers revealed that the membrane domain of the exchanger is responsible for the difference in volume sensitivity between NHE1 and NHE2. Although deletion or point mutation within the first extracellular loop of NHE1 did not affect RVI and alkalinization, point mutations within the corresponding region of NHE2, particularly a region containing aa 41−53, as well as replacement of the N-terminus of NHE2 with the corresponding region of NHE1, rendered NHE2 responsive to the activating effect of cell shrinkage. Thus, the membrane domain plays an important role in the response of the exchanger to cell shrinkage. The data suggest that the putative first extracellular loop of NHE2, but not that of NHE1, may exert an inhibitory influence on hyperosmolarity-induced activation of the exchanger and thereby block RVI.

In hyper- or hypoosmotic medium, cell volume rapidly recovers from shrinkage or swelling through processes named regulatory volume increase (RVI)[1] or regulatory volume decrease (RVD) (*1*−*4*). RVI is usually initiated by net uptake of Na^+ and Cl^-, which is accompanied by osmotically obliged water movement. In several cell types, the uptake of NaCl is mediated via functionally coupled Na^+/H^+ exchanger (NHE) and Cl^-/HCO_3^- exchanger (AE) (*1*−*4*). For example, RVI is impaired in the NHE-deficient mutant cell line AP1 derived from Chinese hamster ovary cells (*5*). Similarly, RVI is impaired in *Xenopus* oocytes expressing NHE but lacking anion exchanger (*6*). However, it can be restored when oocytes are transfected with cDNA of the AE2 anion exchanger (*6*).

NHE catalyzes Na^+ influx coupled with H^+ efflux across the plasma membrane. The NHE family comprises eight known isoforms that are thought to differ in tissue localization, inhibitor potency, and mode of regulation, although they have similar overall structures consisting of the N-terminal membrane catalytic domain (~500 aa) and the C-terminal cytoplasmic regulatory domain (~300 aa) (*7*−*11*). The molecular mechanisms for regulation of some of these NHE isoforms have been extensively studied. However, the mechanism for cell volume-dependent regulation of NHE isoforms remains largely unknown. The Na^+/H^+ exchanger isoform 1 (NHE1), a ubiquitous isoform, is activated in response to cell shrinkage and thus induces a long-lasting cytoplasmic alkalization (see refs *7* and *11* for reviews). In contrast, the same stress inhibits the activity of NHE3 and thereby induces a large cytoplasmic acidification (*12*, *13*). On the other hand, hyperosmolarity does not induce alkalinization in a NHE-deficient mutant cell line, PS120, expressing NHE2 (*13*, *14*) but does so in a different cell line, AP1, expressing NHE2 (*12*). Therefore, these NHE isoforms appear to respond differently to hyperosmotic stress. In these previous studies of NHE isoforms, a change in cell volume has not been measured.

In this study, we measured hyperosmolarity-induced changes in cell height and intracellular pH in PS120 cells expressing NHE1, NHE2, NHE3, or their mutant variants. A change in cell height was used as an index for a change in cell volume of these adherent cells (see Experimental Procedures and refs *15*−*19*). Hyperosmolarity-induced rapid recovery of cell height as well as cytoplasmic alkalinization was observed only in NHE1-expressing cells. Analysis with chimeric and point mutant exchangers has provided evidence suggesting that the N-terminal portion of the transmembrane domain of the exchanger is responsible for the difference in volume sensitivity between NHE1 and NHE2. In NHE2, the first extracellular loop appears to inhibit hyperosmolarity-induced activation of the exchanger and thus block RVI.

† This work was supported by Grant-in-aids on Priority Areas 13142210 and Grant-in-aid 14580664 for Scientific Research from the Ministry of Education, Science, and Culture of Japan and grants from CREST (Core Research for Evolutional Science and Technology) of the Japan Science and Technology Corporation (JST) and the Organization of Pharmaceutical Safety and Research (OPSR) of Japan (Promotion of Fundamental Studies in Health Science). X.S. was supported by the Science and Technology Agency Fellowship of Japan.

* Address correspondence to this author. Phone: 81-6-6833-5012 (ext 2566). Fax: 81-6-6872-7485. E-mail: wak@ri.ncvc.go.jp.

[1] Abbreviations: NHE, Na^+/H^+ exchanger; RVI, regulatory volume increase; pH_i, intracellular pH; EIPA, 5-(*N*-ethyl-*N*-isopropyl)amiloride; HA, hemagglutinin; biotin maleimide, (3-*N*-maleimidylpropionyl)-biocytin; MTSET, 2-(trimethylammonio)ethyl methanethiosulfonate.

10.1021/bi020427d CCC: $25.00
Published on Web 01/03/2003

EXPERIMENTAL PROCEDURES

Materials. Tetramethylrhodamine–dextran and biotin maleimide [3-(*N*-maleimidylpropionyl)biocytin] were purchased from Molecular Probes Inc. MTSET and streptavidin-conjugated agarose were purchased from Toronto Research Chemicals Inc. and Pierce, respectively. The amiloride derivative 5-(*N*-ethyl-*N*-isopropyl)amiloride (EIPA) was a gift from New Drug Research Laboratories of Kanebo, Ltd. (Osaka, Japan). ^{22}NaCl and [7-^{14}C]benzoic acid were purchased from NEN Life Science Products. Rabbit polyclonal antibody (Y-11) against hemagglutinin (HA) epitope was purchased from Santa Cruz Biotechnology, Inc. All other chemicals were of the highest purity available.

Cell Culture and cDNA Transfection. The Na^+/H^+ exchanger deficient cell line PS120 (*20*), provided by Dr. J. Pouysségur (France, Nice), and the corresponding transfectants were maintained in Dulbecco's modified Eagle's medium (Life Technologies, Inc.) containing 25 mM $NaHCO_3$ and supplemented with 7.5% (v/v) fetal calf serum, penicillin (50 units/mL), and streptomycin (50 μg/mL). Cells were maintained at 37 °C in the presence of 5% CO_2. All cDNA constructs were transfected into PS120 cells by the calcium phosphate–DNA coprecipitation technique (*21*), and stable clones were selected by the repetitive H^+-killing selection procedures (*21*).

Construction of NHE Mutant Plasmids. The plasmids carrying cDNAs coding for the Na^+/H^+ exchangers (NHE1 human isoform, NHE2 and NHE3 rat isoforms) were described previously (*14*, *21*). All of the constructs used in this study were produced by a polymerase chain reaction (PCR) based strategy as described (*21*). In this study, we initially introduced a unique restriction site (*Eag*I) corresponding to aa 481 of NHE2 by a PCR-based method. For construction of chimeric exchangers N1N2 and N2N1, DNA fragments corresponding to the C-terminal cytoplasmic domains of NHE1 and NHE2 were produced by PCR using the respective isoform cDNAs as templates and sets of primers containing exogenous restriction sites and incorporated into the *Eag*I/*Xba*I site in NHE2 and the *Acc*I/*Eco*RI site in NHE1 plasmid, respectively. We also employed a similar PCR-based method for construction of other chimeric exchangers between NHE1 and NHE2. For construction of chimeric exchangers of NHE1 whose N-terminal regions were replaced with the corresponding regions of NHE2, we synthesized antisense hybrid primers containing NHE2 regions at the 3′-end and NHE1 regions at the 5′-end. Using these antisense primers and a sense primer annealing to the N-terminus of NHE2, PCR fragments were produced using NHE2 as a template. At the same time, using sense primers complementary to the NHE1 regions of hybrid primers and an antisense primer annealing to NHE1, PCR fragments were produced using NHE1 as a template. These two types of PCR fragments were mixed and subjected to the second PCR reaction. Resultant second PCR products were digested and incorporated into NHE1 cDNA. Chimeric exchangers of NHE2 containing the N-terminal regions of NHE1 were produced in a similar way. Similarly, we produced PCR fragments containing replaced nucleotides for point mutants or nucleotide sequences coding for the influenza virus HA epitope YPYDVPDYAS. These DNA fragments were digested and inserted into appropriate restriction sites in NHE1 and NHE2 plasmids. Inserted DNA fragments were confirmed by sequencing to ensure the fidelity of construction.

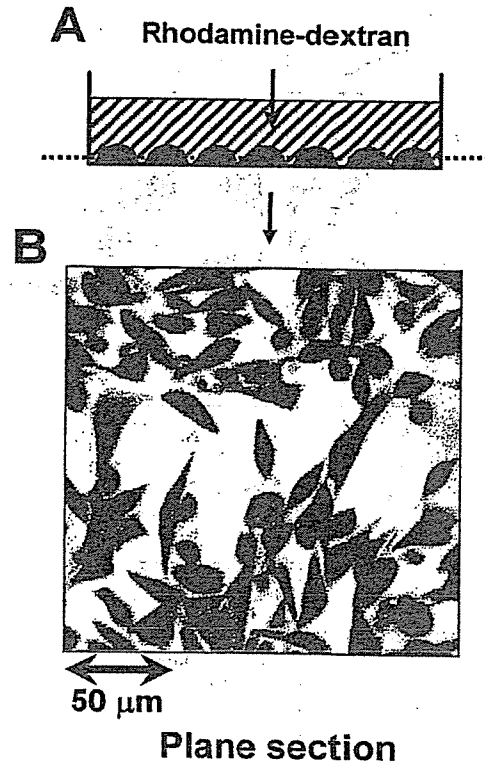

FIGURE 1: Measurement of height of cells attached to a dish. (A) To visualize cell shape, membrane-impermeable tetramethylrhodamine–dextran (0.2 mg/mL) was added to medium. (B) Cells were visualized as nonfluorescent shadows on a confocal fluorescence microscope.

Measurements of Cell Height and Volume. Cells attached to dishes were washed once with 4 mL of serum-free DMEM without phenol red and placed in the same medium containing 0.2 mg/mL membrane-impermeable tetramethylrhodamine–dextran at room temperature to visualize cell shape as a nonfluorescent "shadow" by the fluid labeling method (*22*) (Figure 1). Cells were observed using an MRC-1024 confocal microscope (Bio-Rad) mounted on an Olympus BX50WI fluorescence microscope with a 60× water immersion objective lens. An interface between medium and substratum was determined by taking reflection images (see below). First, we compared hyperosmolarity-induced changes in the height and the volume of the same cells by using the three-dimensional image reconstitution method as described previously (*23*). In these experiments, because image collection took more than 1 min, we used NHE-deficient PS120 cells in which shrinkage was maintained for a relatively long time (see Figure 4A). Before and after induction of shrinkage, 42 optical plane sections (x, y scan at 512 by 512 pixels) were taken along the z-axis at every 0.5 μm (see Figure 1B for an example of one section). Fluorescent images were digitized with 256 intensity levels, and their photometric thresholding was determined empirically with an aid of an imaging software (Scion Image Corp.). Figure 2A,B (lower panels) show contour lines obtained from a cell under control or hyperosmotic conditions. The upper panels represent the vertical sections (x–z) constructed along the dotted lines shown in the lower panels. Volume was calculated by multiplying the sum of x–y areas by the z-axis distance (0.5 μm). Volume and height of the indicated cell were reduced

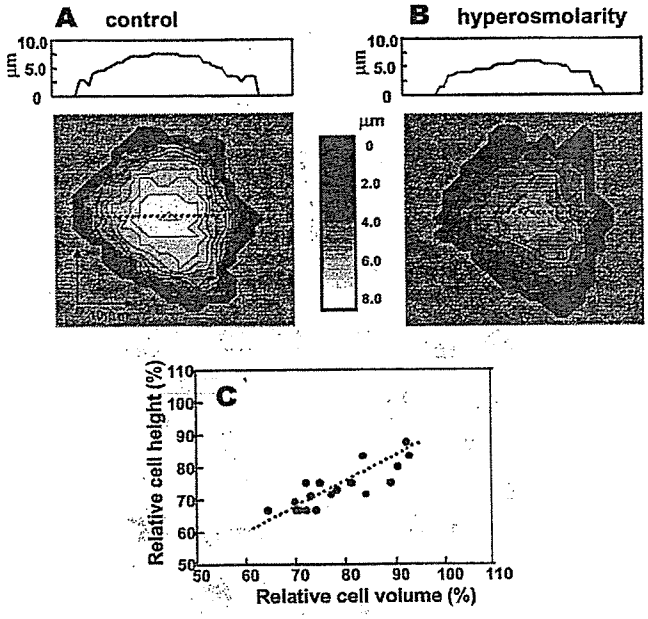

FIGURE 2: Three-dimensional reconstruction from serial optical section images. (A, B) Plane-section images of PS120 cells were taken at 0.5 μm axial intervals under control or hyperosmotic medium (190 mM NaCl) and treated as described under Experimental Procedures. Contour line images were constructed and represented with a gray scale bar. Upper panels show the $x-z$ vertical sections taken along dotted lines shown in lower panels. (C) Relationship between hyperosmotic stress-induced changes in volume and height of 18 cells. Initial values of cell volume and height of individual cells were taken as 100%, and the values of these parameters after shrinkage were normalized to the initial values and plotted in the figure.

from 1.1 to 0.8 pL and 7.5 to 6.0 μm, respectively, upon hyperosmotic stress. Figure 2C shows the relationship between hyperosmolarity-induced changes in volume and height of 18 cells. The initial volume of individual cells varied from 0.7 to 2.0 pL, and the extent of volume change also varied among cells. However, there was significant linear correlation between these two parameters (Figure 2C). Thus, we assume that the change in cell height serves as an index for the change in cell volume at least in our experimental system.

For measurement of time courses of change in cell height, we used 80–90% confluent cells seeded on a 60 mm dish and visualized by fluid labeling as described above. After an $x-y$ plane section image was taken (Figure 1B), a scanning line was chosen in such a way that it passed through near the center of more than five nonoverlapping cells. Vertical cross-section images of cells were reconstructed from scans at that line taken stepwise at every 0.5 μm over a 20 μm focus range (see Figure 3). At the same time, reflection images were taken to visualize an interface between medium and substratum (see dotted lines in Figure 3). Cell edges were determined by an image processing software (Bio-Rad). For each batch of cells expressing individual NHE variants, measurement of cell height change was repeated at least three times, and a representative result is shown in the figure. For each time point, we plotted means ± SD of data from five to seven cells having a cell height above 5 μm (see Figures 3 and 6). Production of a vertical image from line scans usually took about 10 s. We thus used the midpoint of this period for the plot of cell height change. Student's t test was used to evaluate the statistical significance of the difference between cell heights at 30 s and 10 min or later after addition of hyperosmotic medium, and a probability value (P) of less than 0.05 was considered to be significant.

Measurements of pH_i Change and $^{22}Na^+$ Uptake. A change in pH_i was estimated from the distribution of [^{14}C]benzoic acid as described previously (*21*). The stable transfectants grown to confluence in 24-well dishes were serum-depleted for 5 h to maintain the exchanger in the resting state. Cells were further incubated for 1 h at 37 °C in a serum-free, bicarbonate-free DMEM buffered with 20 mM Hepes/Tris (pH 7.0). Cells were then placed for the indicated time in the same medium containing 7 kBq of [^{14}C]benzoic acid/mL with or without 200 mM sucrose. Cells were then rapidly washed four times with ice-cold PBS and solubilized in 0.1 N NaOH, and the ^{14}C radioactivity was counted. Student's t test was used to evaluate the significance of the difference between pH_is before and after addition of hyperosmotic medium, and a probability value (P) of less than 0.05 was considered to be significant.

The $^{22}Na^+$ uptake activity at an acidic pH_i (<6.0) was measured by the NH_4Cl prepulse method as described previously (*21*). Uptake activity was normalized by protein concentration measured by the bicinchoninic assay system (Pierce Chemical Co.) using bovine serum albumin as a standard.

Labeling with Biotin Maleimide. Biotin maleimide labeling of the NHE1 mutant molecules was carried out as described previously (*24*). Briefly, confluent cells were washed twice with PBSCM (phosphate-buffered saline containing 0.1 mM $CaCl_2$ and 1 mM $MgCl_2$) and incubated with or without 5 mM 2-(trimethylammonio)ethyl methanethiosulfonate (MTSET) for 30 min at room temperature. Cells were washed twice with PBSCM and then incubated with 0.5 mM biotin maleimide for 30 min at room temperature. Cells were washed once with PBSCM containing 1% 2-mercaptoethanol and once with PBSCM and collected by centrifugation. Cells were solubilized with lysis buffer containing 1% Triton X-100, 150 mM NaCl, 20 mM Hepes/Tris (pH 7.4), 1 mM PMSF, and 1 mM benzamidine. After centrifugation, the supernatant was mixed with streptavidin–agarose beads, and the mixture was incubated for 1 h at 4 °C with rotation. Agarose beads were washed five times with lysis buffer and then mixed with SDS–PAGE loading buffer containing 3% SDS. Proteins were eluted from beads by boiling for 10 min at 100 °C, separated on an 8.5% acrylamide gel by SDS–PAGE, and subjected to immunoblot analysis with HA antibody. The blots were visualized by the ECL detection system (Amersham Pharmacia Biotech).

RESULTS

Cell Height Change in Transfectants Expressing Wild-Type Exchangers. Figure 3 shows a typical time-dependent change in cell height of NHE1 transfectants upon exposure to hyperosmotic medium containing 190 mM NaCl and 20 mM $NaHCO_3$. As shown in the figure, NaCl at a concentration 50 mM in excess over the physiological level induced fast cell shrinkage, followed by slower recovery. Figure 4 shows summary data for these experiments. In NHE1 transfectants, 190 mM NaCl induced a 20–30% decrease in cell height, followed by a relatively rapid recovery that was completely

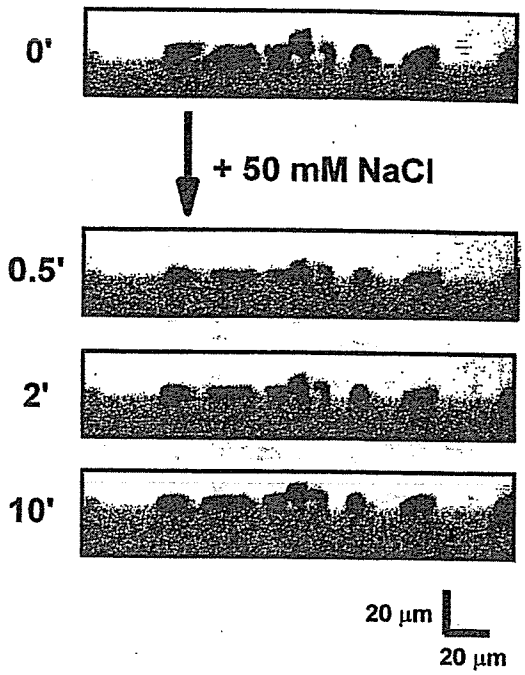

FIGURE 3: Change in cell height induced by hyperosmotic stress. The vertical images of cells expressing NHE1 were observed before and after exposure to high NaCl medium (final NaCl concentration, 190 mM). The experiment was done in serum-free DMEM containing 0.2 mg/mL tetramethylrhodamine–dextran, 20 mM $NaHCO_3$, and 20 mM Hepes/NaOH (pH 7.4). The dotted line in each panel represents the reflection line.

inhibited by the NHE inhibitor EIPA (Figure 4B). We also observed that 100 mM sorbitol or mannitol induced a similar decrease in cell height of NHE1 transfectants, followed by an EIPA-inhibitable recovery [relative cell height, 77.9 ± 5.7% and 97.8 ± 10.6% ($n = 15$, $P < 0.05$) at 1 and 15 min after sorbitol addition and 69.2 ± 12.1% and 93.3 ± 5.7% ($n = 10$, $P < 0.05$) at 1 and 15 min after mannitol addition, respectively]. In this study, we mainly used NaCl instead of sorbitol or mannitol, because the latter was difficult to be mixed rapidly after the addition. The spontaneous recovery in cell height was not observed in exchanger-deficient PS120 cells (Figure 4A), although the height of these cells was rapidly recovered when they were again placed in isoosmotic medium (data not shown). We observed a slower but significant recovery of cell height (more than 90%) in CCL-39 cells with an endogenous NHE1 that exhibited about 10 times less activity compared with NHE1-overexpressing PS120 cells (data not shown). These data suggest that NHE1 is required for volume recovery, consistent with a previous finding that the NHE-deficient mutant cell line AP1 did not exhibit RVI, although the AP1 experiment was done using a different experimental protocol (*5*). In contrast to NHE1 transfectants, NHE2 or NHE3 transfectants did not exhibit a rapid recovery of cell height (Figure 4C,D), although these cells exhibit high Na^+/H^+ exchange activity (see legend to Figure 4). Thus, NHE2 and NHE3 did not confer to PS120 cells the ability to respond to cell volume change.

Cell Height Change in Transfectants Expressing Chimeric or Mutant Exchangers. The results described above show clear differences in the responses of NHEs 1 to 3 to hyperosmotic stress. Because amino acid sequences of NHE1 and NHE2 are fairly homologous to each other (70% amino acid similarity or 53% amino acid identity), we hypothesized that the difference in the osmotic sensitivity arises from the structural difference in the limited regions of these exchangers. We constructed various chimeric exchangers between NHE1 and NHE2 and examined osmotic response in cells expressing them (Figures 5 and 6). In transfectants with two chimeras, E1E2 and E2E1, in which the C-terminal cytoplasmic domains of NHE1 and NHE2 were exchanged with the corresponding domains of NHE2 and NHE1, respectively, recovery of the height was observed in cells expressing E1E2 but not in cells expressing E2E1 (Figure 7A). The result suggests that the N-terminal transmembrane domain is

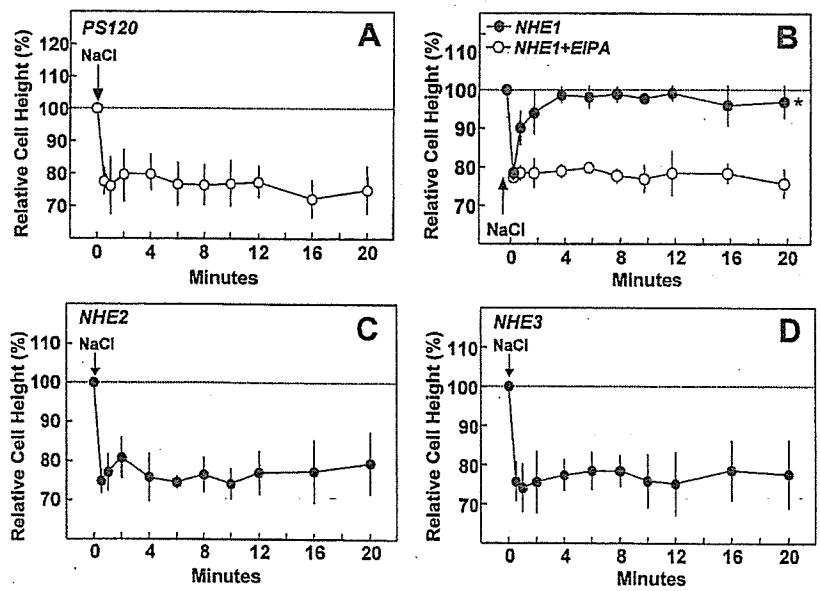

FIGURE 4: Time courses of hyperosmolarity-induced changes in cell height. Changes in cell height were measured in PS120 cells (A) or PS120 cells expressing NHE1 (B), NHE2 (C), or NHE3 (D) placed in serum-free DMEM containing 0.2 mg/mL tetramethylrhodamine–dextran, 20 mM $NaHCO_3$, and 20 mM Hepes/NaOH (pH 7.4). NaCl was added to a final concentration of 190 mM at the time indicated by arrows. In one experiment, medium contained 0.1 mM EIPA (B, open circle). Values are means ± SD of data obtained from five to seven cells (*, $P < 0.05$ versus the cell height at 30 s). EIPA-sensitive $^{22}Na^+$ uptake activity of cells expressing NHE1, NHE2, or NHE3 was 22.4 ± 1.8, 11.1 ± 0.2, or 25.0 ± 0.5 ($n = 3$) nmol mg^{-1} min^{-1}, respectively.

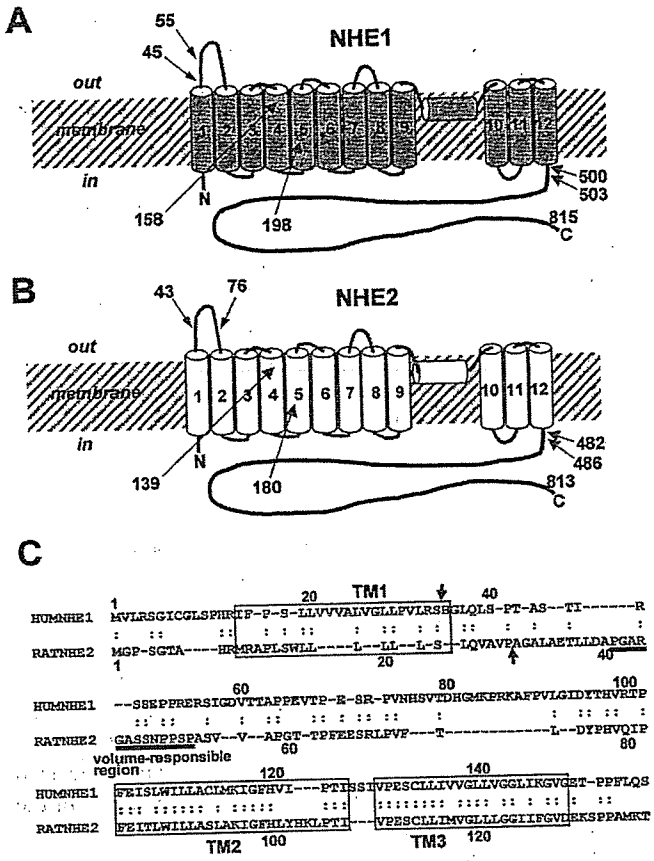

FIGURE 5: Structural models and amino acid sequences of NHE1 and NHE2. (A, B) Topology models for NHE1 and NHE2 deduced from the previous data (*24*). Numbers show approximate positions of amino acid residues corresponding to the junctions between NHE1 and NHE2 in chimeric exchangers. (C) Amino acid sequence alignment between NHE1 and NHE2. TM1−3 show putative transmembrane spanning segments. The identified volume-responsible region of NHE2 is underlined. Arrows indicate the most likely cleavage sites in NHE1 or NHE2 for signal peptidase.

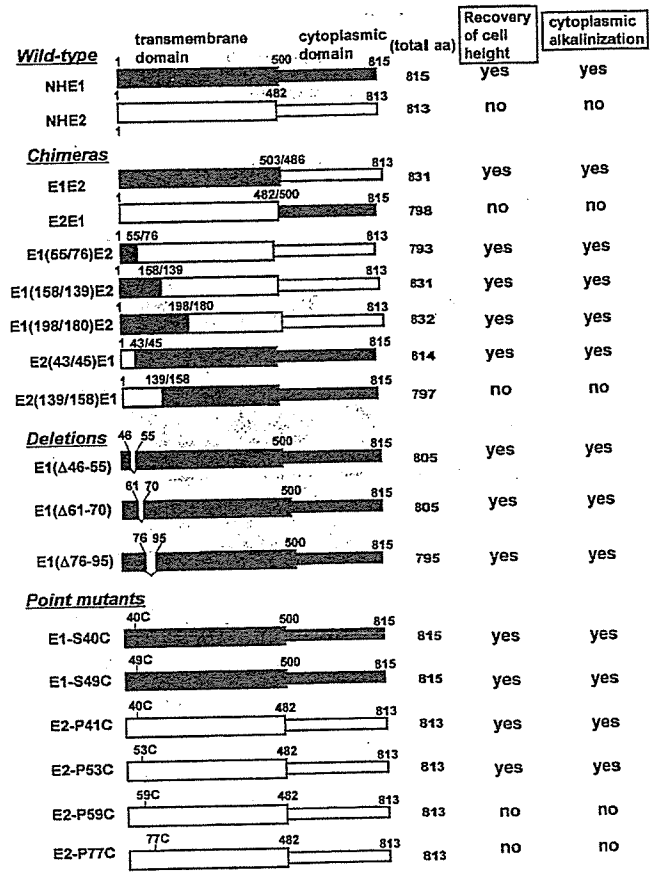

FIGURE 6: Constructs of various NHE variants and their responsiveness to hyperosmotic stress. Chimeric and mutant NHE constructs used in this study are shown. However, some point mutant constructs for NHE2 (P41A, G45C, S48C, P50C, A54C, F72C, and P77A) are not shown (however, see Figure 7). "Yes" on the right indicates the occurrence of significant ($P < 0.05$) recovery of cell height or cytoplasmic alkalinization, while "no" indicates the absence of significant changes in these parameters.

responsible for the differential osmotic responses of these isoforms.

We prepared more than 40 different chimeras involving the transmembrane domains of NHE1 and NHE2. Unfortunately, most of them exhibited no or low exchange activity, which may be due to structural distortion caused by chimera formation. However, recovery of the height was observed in cells expressing E1(55/76)E2 and E2(43/45)E1, in which the N-terminal regions of NHE2 (aa 1−75) and NHE1 (aa 1−44) were replaced by the corresponding regions of NHE1 (aa 1−55) and NHE2 (aa 1−43), respectively (Figure 7B). Recovery of the height of more than 90% was also observed in cells expressing other chimeras, E1(158/140)E2 and E1(198/180)E2 [chimeras are designated as in E1(55/76)E2 and E2(43/45)E1] (data not shown). In contrast, it was not observed in cells expressing E2(139/158)E1, although this mutant exhibited high exchange activity. These results suggest that the N-terminus, in particular, the first extracellular portion of exchanger, is important for the difference in the osmotic responses of NHE1 and NHE2.

We considered two possibilities: (i) the N-terminus of NHE1 functions as a positive regulatory element that renders the chimeric exchangers sensitive to hyperosmotic stress or (ii) the N-terminus of NHE2 functions as a negative regulatory element that renders the chimeric exchangers insensitive. To help to discriminate between these possibilities, we introduced deletion or point mutations into the N-terminus of NHE1 or NHE2. Recovery of the height was observed in cells expressing several deletion mutants, Δ76−95, Δ61−70, and Δ46−55, or point mutants (S40C and S49C) of NHE1 (Figure 7C; data not shown for some mutants). On the other hand, several point mutations in NHE2, i.e., P41C, P50C, and P53C, rendered the exchanger responsive to cell shrinkage, while P59C and P77A did not (Figure 7D; not shown for P50C). Unfortunately, other mutants, such as E1(Δ46−95) and E2(Δ44−75), could not be used in these experiments because of their low expression in cells. The data appear to be consistent with the view that the N-terminus of NHE2 has an inhibitory effect on recovery of cell height.

Hyperosmolarity-Induced Change in Intracellular pH. In the absence of $NaHCO_3$, we observed that hyperosmotic stress such as 200 mM sucrose (Figure 8A) or a concentration of NaCl 100 mM in excess over the physiological level (Figure 8F) induced an EIPA-sensitive cytoplasmic alkalinization in NHE1 transfectants. In contrast, hyperosmotic stress induced cell acidification in NHE2 transfectants (Figure 8A). Since such acidification was also observed in nontransfected PS120 cells, we consider that this acidification is due to intracellular acid production or activation of some H^+-

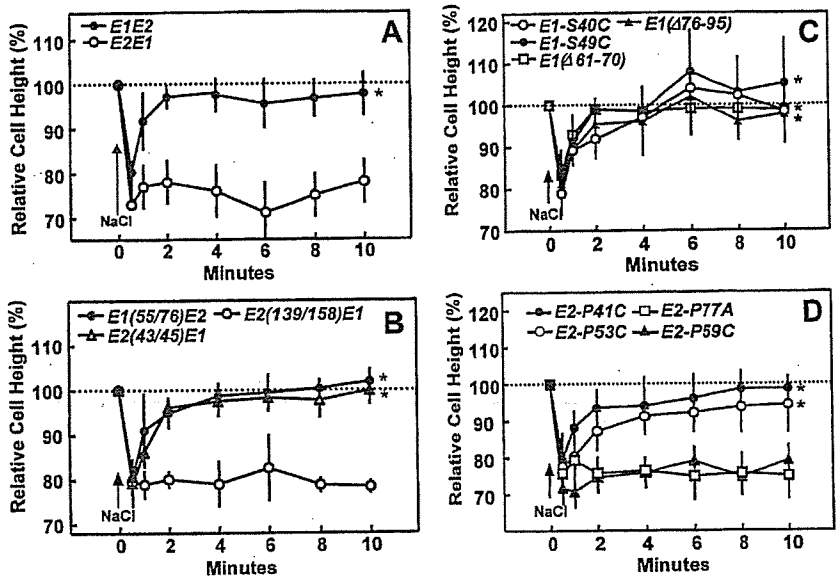

FIGURE 7: Time courses of hyperosmolarity-induced changes in the height of cells expressing various NHE variants. Time courses of cell height change were measured as in Figure 3 in PS120 cells expressing chimeric (A) and deletion or point mutant exchangers for NHE1 (C) or NHE2 (D) after exposing them to 190 mM NaCl at the time indicated by the arrows. EIPA-sensitive $^{22}Na^+$ uptake activities in cells expressing these mutant exchangers ranged between 8 and 27 nmol mg^{-1} min^{-1} (see also Figure 6E for activities of mutant exchangers). Values are means ± SD of data obtained from five to seven cells (*, $P < 0.05$ versus the cell height at 30 s).

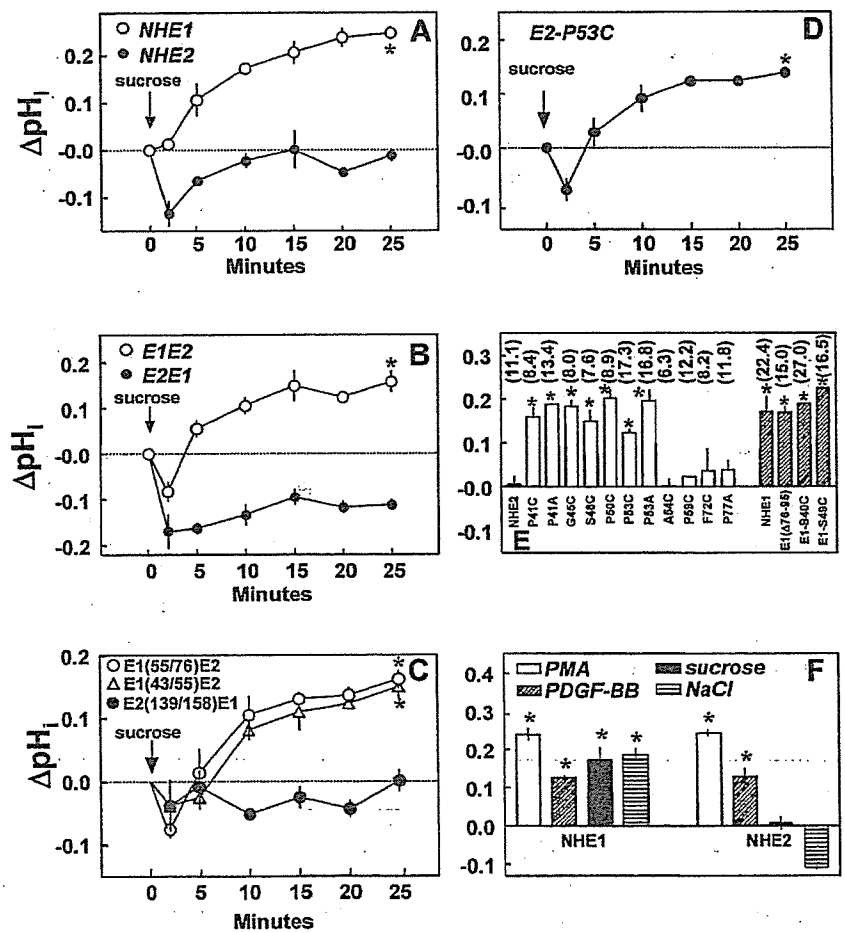

FIGURE 8: Hyperosmolarity-induced cytoplasmic alkalinization in PS120 cells expressing various NHE variants. Time courses of pH_i change were followed in PS120 cells expressing NHE1 or NHE2 (A), E1E2 or E2E1 (B), E1(55/76)E2, E2(43/55)E1, or E2(139/158)E1 (C), or E2-P53C (D) after exposing them to 200 mM sucrose at the time indicated by the arrows. (E) Changes in pH_i in cells expressing NHE2 (open bars) or NHE1 (closed bars) mutants were measured 15 min after the addition of 200 mM sucrose. Values are means ± SD of three determinations. The numbers in parentheses are EIPA-sensitive $^{22}Na^+$ uptake activities (nmol mg^{-1} min^{-1}) of the transfectants carrying respective NHE variants. (F) Effects of various stimuli on pH_i. Cells expressing NHE1 or NHE2 were treated with 1 μM PMA, 100 ng/mL PDGF-BB, 200 mM sucrose, or 240 mM NaCl for 15 min. Values are means ± SD of three determinations (*, $P < 0.05$ versus before stimulation). Resting pH_i before stimulation was in the range of 7.1−7.3 in these experiments.

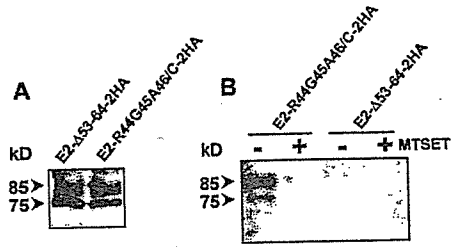

FIGURE 9: Surface labeling of cysteine residues incorporated into the volume-sensitive region of NHE2. Cells expressing HA-tagged NHE2 mutants (E2-Δ54-63-2HA or E2-R44G45A46/C-2HA), which had been treated with or without 5 mM MTSET, were incubated with biotin maleimide, solubilized with the lysis buffer, and then treated with streptavidin−agarose, as described under Experimental Procedures. Total cell lysates (20 μg each) (A) or the proteins recovered with streptavidin−agarose (B) were separated by SDS−PAGE, and exchanger proteins were visualized by immunoblot analysis with HA antibody.

entry pathways caused by cell shrinkage. In NHE2 transfectants, pH_i sometimes recovered to the original level after the initial transient acidification induced by sucrose addition. The latter pH_i recovery was inhibited by EIPA (data not shown). We consider that this recovery was due to activation of NHE2 in response to shrinkage-induced cell acidification, which probably was not sufficient to induce recovery of cell height. In contrast to hyperosmolarity, other stimuli such as PMA and PDGF induced significant cytoplasmic alkalinization in both NHE1 and NHE2 transfectants (Figure 8F), indicating that NHE2 is indeed activated by these stimuli.

We measured the effect of hyperosmolarity on pH_i change in cells expressing various chimeric or point mutant exchangers. Hyperosmolarity induced cytosolic alkalinization in all of the mutant transfectants that exhibited recovery of cell height but not in those showing little such recovery (Figure 8A−E; see also Figure 6). This good correlation between changes in cell height and pH_i supports the view that activation of NHE is required for recovery of cell height. Figure 8E shows the effects of point mutations in the first extracellular portion of the exchanger on the hyperosmolarity-induced cytoplasmic alkalinization in transfectants. Some point mutants of NHE2 (P41C, P41A, G45C, S48C, P50C, P53C, and P53A), but not others (A54A, P59C, F72C, and P77A), induced cytoplasmic alkalinization, suggesting that the region aa 41−53 is important for the response of NHE2 to a change in cell height.

Sidedness of the Volume-Sensitive Region of NHE2. We examined the sidedness of the hyperosmolarity-sensitive region of NHE2 with respect to the membrane by analyzing accessibility of incorporated cysteines to externally applied membrane-impermeable SH reagents. We used cells expressing E2-R44C/G45C/A46C-2HA (Arg44, Gly45, and Ala46 of NHE2 were substituted by cysteines, with the C-terminal end tagged with two HA epitopes). We used cells expressing E2-Δ53-64-2HA (aa 53−64 of NHE2 was deleted) as the control for the cysteine accessibility analysis. Both HA-tagged NHE2 mutants were expressed at similar levels (Figure 9A). For each mutant, we observed two forms of the exchanger with high (85 kDa) or low (75 kDa) molecular mass that are thought to be the O-glycosylated mature or nonglycosylated immature form, respectively (*25*). The cysteine-containing E2-R44C/G45C/A46C-2HA was significantly labeled with externally applied biotin maleimide but not labeled when cells had been pretreated with externally applied membrane-impermeable SH reagent MTSET (Figure 9B). In contrast, E2-Δ53-64-2HA was not labeled with external biotin maleimide even in the absence of MTSET. The data demonstrate that cysteines incorporated into the region of NHE2 involved in volume regulation are exposed on the extracellular side, which is consistent with our previous finding that the corresponding region in NHE1 forms part of the first extracellular loop (*24*).

DISCUSSION

In this study, we measured the hyperosmolarity-induced change in the height of adherent cells expressing various NHE variants by using confocal microscopy and extracellular fluid labeling with a fluorescent dye. Our initial study, in which we compared hyperosmolarity-induced changes in the height and the volume of the same cells measured by the three-dimensional image reconstitution method, suggested that there was significant linear correlation between these two parameters (Figure 2C). We thus assumed that the change in the height of adherent cells serves as a convenient measure of the change in cell volume at least in our experimental system.

The well-documented ion transport systems participating in RVI are the $Na^+/K^+/2Cl^-$ cotransporter and a combination of Na^+/H^+ and Cl^-/HCO_3^- exchangers (*1*−*4*). Coupled activities of the latter exchangers have been shown to be responsible for RVI in many cell types. Our study revealed that cells expressing NHE1 restore their cell height from the hyperosmolarity-induced shrinkage in an EIPA-sensitive manner (see Figures 3 and 4B). Furthermore, in nontransfected PS120 cells lacking NHE activity, a similar recovery of cell height was not observed at least during an initial 20 min after cell shrinkage. Thus, NHE1, presumably with the Cl^-/HCO_3^- exchanger, may play a major role in RVI in our cell system, while the $Na^+/K^+/2Cl^-$ cotransporter contributes minimally.

In contrast to cells expressing NHE1, cells expressing NHE2 or NHE3 did not recover their cell height rapidly after shrinkage (see Figure 4), suggesting that they are not responsive to a change in cell volume. Consistent with this finding, hyperosmolarity induced cytoplasmic alkalinization in cells expressing NHE1 but not in cells expressing NHE2 or NHE3 (Figure 8; see also refs *13* and *14*). The data suggest that these NHE isoforms may possess regions conferring different volume sensitivity. We used a chimera strategy involving NHE1 and NHE2 to search for such regions. Cells expressing a chimeric exchanger, E1E2, showed recovery of cell height and cytoplasmic alkalinization, while a reciprocal chimeric exchanger, E2E1, did not (Figure 7A). Thus, the transmembrane domain of the exchanger is important for the shrinkage-induced activation of the exchanger. This result appears to be consistent with a previous finding that an NHE1 mutant (Δ566) having a large deletion of the C-terminal cytoplasmic domain is activated in response to hyperosmotic stress (*26*).

Recovery of cell height and cytoplasmic alkalinization were observed in cells expressing several other chimeric exchangers, E1(55/76)E2, E1(158/139)E2, and E1(198/180)E2, in which the N-terminus of NHE2 was replaced by the corresponding regions of NHE1 but not in cells express-

ing a reciprocal chimeric exchanger, E2(139/158)E1 (see Figures 7B and 8C and Results). These data suggest that the N-termini of exchangers are important for the differential responses of NHE1 and NHE2. The result shown in Figure 9 suggests that the region (aa 25−85) of NHE2 corresponding to aa 35−110 of NHE1 is exposed on the external side. We do not know whether the N-terminus of NHE2 is cleaved off or not as the signal peptide. If it is not cleaved off, the NHE2 region (aa 25−85) is mapped to the first extracellular loop (see below). Interestingly, amino acid sequences of the N-termini of NHE1 and NHE2 are very different (see Figure 5C), despite the fact that the remaining portions of the transmembrane domain of both isoforms are highly homologous (~70% amino acid identity). Such divergence in the sequence may provide a structural basis for the observed functional difference between the two isoforms.

Recovery of cell height and cytoplasmic alkalinization were observed in cells expressing several deletion or point mutants in the first extracellular loop of NHE1, Δ76−95, Δ61−70, Δ46−55, S40C, and S49C (see Figures 7C and 8E). In addition, these two events were observed in a chimeric exchanger, E2(43/55)E1, in which the N-terminal 44 amino acids of NHE1 were replaced by the corresponding 43 amino acids of NHE2 (see Figures 7B and 8C). These data suggest that the N-terminal region (aa 1−95) of NHE1 encompassing the cytosolic N-tail, the first transmembrane segment, and the first extracellular loop is not involved in the volume-sensing mechanism of NHE1.

In NHE2, not as in NHE1, mutations in the first extracellular loop caused a remarkable change in the volume-dependent regulation of exchange activity; surprisingly, some mutations at single residues introduced into the N-terminus (aa 41−53) rendered the exchanger activatable by cell shrinkage, although other mutations did not (Figures 7B and 8E). Furthermore, a chimeric exchanger, E2(139/158)E1, was not activated by cell shrinkage, although E2(43/55)E1 showed recovery of cell height and alkalinization as noted above. Together, these results suggest that the first extracellular loop of NHE2 exerts an inhibitory influence on shrinkage-induced activation of the exchanger and thus blocks RVI. Such an inhibitory action of the first extracellular loop of NHE2 and the absence of regulatory influence of the corresponding segment of NHE1 may explain why several NHE2 chimeras carrying the N-terminal NHE1 segments, i.e., E1(55/76)E2, E1(158/139)E2, and E1(198/180)E2, are activated by cell shrinkage.

According to an algorithm for prediction of signal sequence, the NHE isoforms NHE1−7 were predicted to contain signal peptides.[2] Indeed, it has been reported on the basis of in vitro translation experiments that the N-termini of NHE3 (*27*) and NHE1 (*28*) are cleaved off as signal peptides. However, we previously found that Cys-8 in the N-tail of NHE1 was labeled with biotin maleimide only after cells were permeabilized, suggesting that the N-tail of NHE1 is retained in the cytosol at least partly (*24*). Therefore, we are not certain about the extent to which the mature NHE1 expressed in the plasma membrane retains the N-tail in the cytosol. Further experiments such as determination of the N-terminal amino acid sequences of mature NHE isoforms would be required to obtain an unambiguous conclusion. It should be noted, however, that the predicted cleavage sites in NHE1 and NHE2 are located in regions N-terminal to the functionally important regions identified in this study (see Figure 5C).

We previously showed that surface biotinylation of substituted cysteine residues in the first extracellular loop of NHE1 was not uniform (*24*), suggesting that the loop is not completely exposed externally and may form a compact folded structure. This loop may not functionally interact with other important region(s) of the exchanger, because deletions within it did not significantly influence the shrinkage-induced activation of NHE1 (see above). In contrast, the first extracellular loop of NHE2 appears to functionally interact with other region(s) of the exchanger, because this region of NHE2 is highly mutation-sensitive and such mutations render the exchanger sensitive to cell shrinkage (see above). The first extracellular loop of NHE2 could interact with other region(s) of the transmembrane domain of the exchanger or other adjacent proteins. In this context, it is interesting to note that, in the cystic fibrosis transmembrane conductance regulator, disease-associated point mutations in extracellular loops 1, 2, and 4 exert a significant influence on the stability of the channel pore (*29*).

We currently have little information regarding how NHE1 and NHE2 with mutations in the first extracellular loop are activated in response to cell shrinkage. It is possible that the exchanger directly senses a change in membrane strain imposed by cell shrinkage. One example of membrane proteins that directly sense membrane strain is the bacterial stretch-activated channel MscL (*30*, *31*). Furthermore, two recent studies have shown that an osmoregulated ABC transporter OpuA of *Lactococcus latis* (*32*) and a betanine carrier BetP of *Corynebacterium glutamicum* (*33*) are activated in response to hyperosmotic stress when purified proteins were reconstituted in proteoliposomes that are devoid of all other cellular proteins, strongly suggesting that transporter activation by a transmembrane osmotic gradient is mediated via changes in membrane properties such as membrane strain, curvature stress, or protein−lipid interactions. On the other hand, previous literature also reported that cell shrinkage-induced activation of NHE1 occurs via intracellular events involving several families of protein kinases (*34*−*37*) or a Cl^--dependent, G-protein-mediated process (*38*) or Ca^{2+}/calmodulin-dependent process (*39*). It is not clear how these intracellular events are related to the membrane events that we have seen in this study.

In summary, we presented evidence that the first extracellular loop is responsible for the differential volume sensitivity of NHE1 and NHE2. The data suggest that the first extracellular loop of NHE2, but not that of NHE1, may exert an inhibitory influence on hyperosmolarity-induced activation of the exchanger. Thus, the exchanger may not be activated simply through intracellular signaling events caused by cell shrinkage. Our present findings provide new information regarding cell shrinkage-induced activation of the Na^+/H^+ exchanger.

REFERENCES

1. Demaurex, N., and Grinstein, S. (1994) *J. Exp. Biol. 196*, 389−404.
2. Grinstein, S., and Foskett, J. K. (1990) *52*, 399−414.

[2] Prediction was made on the World Wide Web.

3. Haussinger, D. (1996) *Biochem. J. 313*, 697−710.
4. Lang, F., Busch, G. L., Ritter, M., Volkl, H., Wakdegger, S., Gulbins, E., and Haussinger, D. (1998) *Physiol. Rev. 78*, 247−306.
5. Rotin, D., and Grinstein, S. (1989) *Am. J. Physiol. 257*, C1158−C1165.
6. Jiang, L., Chernova, M. N., and Alper, S. L. (1997) *Am. J. Physiol 272*, C191−C202.
7. Orlowski, J., and Grinstein, S. (1997) *J. Biol. Chem. 272*, 22373−22376.
8. Orlowski, J., Kandasamy, R. A., and Shull, G. E. (1992) *J. Biol. Chem. 267*, 9331−9339.
9. Sardet, C., Franchi, A., and Pouysségur, J. (1989) *Cell 56*, 271−280.
10. Tsé, C. M., Levine, S. A., Yun, C. H. C., Montrose, M. H., Little, P. J., Pouysségur, J., and Donowitz, M. (1993) *J. Biol. Chem. 268*, 11917−11924.
11. Wakabayashi, S., Shigekawa, M., and Pouysségur, J. (1997) *Physiol. Rev. 77*, 51−74.
12. Kapus, A., Grinstein, S., Wasan, S., Kandasamy, R., and Orlowski, J. (1994) *J. Biol. Chem. 269*, 23544−23552.
13. Nath, S. K., Hang, C. Y., Levine, S. A., Yun, C. H. C., Montrose, M. H., Donowitz, M., and Tsé, C. M. (1996) *Am. J. Physiol. 270*, G431−G441.
14. Kobayashi, Y., Pang, T., Iwamoto, T., Wakabayashi, S., and Shigekawa, M. (2000) *Pfluegers Arch. 439*, 455−462.
15. Roy, G., and Sauvé, R. (1987) *J. Membr. Biol. 100*, 83−96.
16. Crowe, W. E., and Wills, N. K. (1991) *Pfluegers Arch. 419*, 349−357.
17. van Driessche, W., Smet, P. D., and Raskin, G. (1993) *Pfluegers Arch. 425*, 164−171.
18. Wong, C.-S., Lui, P.-Y., and Kong, S.-K. (1999) *Bioimages 7*, 113−120.
19. Wang, Z., Mitsuiye, T., Rees, S. A., and Noma, A. (1997) *J. Gen. Physiol. 110*, 73−82.
20. Pouysségur, J., Sardet, C., Franchi, A., L'Allemain, G., and Paris, S. (1984) *Proc. Natl. Acad. Sci. U.S.A. 81*, 4833−4837.
21. Wakabayashi, S., Fafournoux, P., Sardet, C., and Pouysségur, J. (1992) *Proc. Natl. Acad. Sci. U.S.A. 89*, 2424−2428.
22. Murakami, T., Ono, M., and Ishikawa, H. (1993) *Bioimages 1*, 1−8.
23. Sato, H., Delbridge, L. M. D., Blatter, L. A., and Bers, D. M. (1996) *Biophys. J. 70*, 1494−1504.
24. Wakabayashi, S., Pang, T., Su, X., and Shigekawa, M. (2000) *J. Biol. Chem. 275*, 7942−7949.
25. Tsé, C. M, Levine, S. A., Yun, C. H. C., Khurana, S., and Donowitz, M. (1994) *Biochemistry 33*, 12954−12961.
26. Bianchini, L., Kapus, A., Lukacs, G., Wasan, S., Wakabayashi, S., Pouysségur, J., Yu, F. H., Orlowski, J., and Grinstein, S. (1995) *Am. J. Physiol. 269*, C998−C1007.
27. Zizak, M., Cavet, M. E., Bayle, D., Tsé, C.-M., Hallen, S., Sachs, G., and Donowitz, M. (2000) *Biochemistry 39*, 8102−8112.
28. Miyazaki, E., Sakaguchi, M., Wakabayashi, S., Shigekawa, M., and Mihara, K. (2001) *J. Biol. Chem. 276*, 49221−49227.
29. Hämmerle, M. M., Aleksandrov, A. A., and Riordan, J. R. (2001) *J. Biol. Chem. 276*, 14848−14854.
30. Sukharev, S. I., Blount, P., Martinac, B., and Kung, C. (1997) *Annu. Rev. Physiol. 59*, 633−657.
31. Wood, J. M. (1999) *Microbiol. Mol. Biol. Rev. 63*, 230−262.
32. van der Heide, T., and Poolman, B. (2000) *Proc. Natl. Acad. Sci. U.S.A. 97*, 7102−7106.
33. Rübenhagen, R., Rönsch, H., Jung, H., and Krämer, R. (2000) *J. Biol. Chem. 275*, 735−741.
34. Wesselborg, S., Bauer, M. K. A., Vogt, M., Schmitz, M. L., and Schulze-Osthoff, K. (1997) *J. Biol. Chem. 272*, 12422−12429.
35. Gatsios, P., Terstegen, L., Schliess, F., Haussinger, D., Kerr, I. M., Heinrich, P. C., and Graeve, L. (1998) *J. Biol. Chem. 273*, 22962−22968.
36. Kapus, A., Szaszi, K., Sun, J., Rizoli, S., and Rotstein, O. D. (1999) *J. Biol. Chem. 274*, 8093−8102.
37. Shrode, L. D., Klein, J. D., O'Neill, C., and Putnum, R. W. (1995) *Am. J. Physiol. 269*, C257−C266.
38. Hogan, E. M., Davis, B. A., and Boron, W. F. (1997) *J. Gen. Physiol. 110*, 629−639.
39. Bertrand, B., Wakabayashi, S., Ikeda, T., Pouysségur, J., and Shigekawa, M. (1994) *J. Biol. Chem. 269*, 13703−13709.

BI020427D

Am J Physiol Heart Circ Physiol 285: H38–H46, 2003.
First published March 6, 2003; 10.1152/ajpheart.01037.2002.

15-Deoxy-$\Delta^{12,14}$-prostaglandin J_2 and laminar fluid shear stress stabilize c-IAP1 in vascular endothelial cells

Yoji Taba,[1,2] Megumi Miyagi,[1,2] Yoshikazu Miwa,[1] Hiroyasu Inoue,[3] Fumi Takahashi-Yanaga,[1] Sachio Morimoto,[1] and Toshiyuki Sasaguri[1]

[1]*Department of Clinical Pharmacology, Graduate School of Medical Sciences, Kyushu University, Fukuoka 812-8582;* [2]*Third Department of Internal Medicine, University of the Ryukyus School of Medicine, Okinawa 903-0215;* [3]*Department of Pharmacology, National Cardiovascular Center Research Institute, Osaka 565-8565, Japan*

Submitted 2 December 2002; accepted in final form 27 February 2003

Taba, Yoji, Megumi Miyagi, Yoshikazu Miwa, Hiroyasu Inoue, Fumi Takahashi-Yanaga, Sachio Morimoto, and Toshiyuki Sasaguri. 15-Deoxy-$\Delta^{12,14}$-prostaglandin J_2 and laminar fluid shear stress stabilize c-IAP1 in vascular endothelial cells. *Am J Physiol Heart Circ Physiol* 285: H38–H46, 2003. First published March 6, 2003; 10.1152/ajpheart.01037.2002.—Laminar shear stress strongly inhibits vascular endothelial cell apoptosis by unknown mechanisms. We reported that shear stress stimulates endothelial cells to produce 15-deoxy-$\Delta^{12,14}$-prostaglandin J_2 (15d-PGJ_2) by elevating the expression level of lipocalin-type prostaglandin D synthase. To investigate the role of 15d-PGJ_2 produced in the vascular wall, we examined the effect of 15d-PGJ_2 on endothelial cell apoptosis. We induced apoptosis in human umbilical vein endothelial cells (HUVECs) by growth factor deprivation. 15d-PGJ_2 strongly inhibited DNA ladder formation, nuclear fragmentation, and caspase-3-like activity in HUVECs. To elucidate the mechanism by which 15d-PGJ_2 inhibits endothelial cell apoptosis, we examined expression of the inhibitor of apoptosis proteins (IAP) cellular-IAP1 (c-IAP1), c-IAP2, x-linked IAP, and survivin in HUVECs. In parallel with the inhibition of apoptosis, 15d-PGJ_2 elevated the expression level of c-IAP1 protein in a dose- and time-dependent manner without changing the mRNA level. Laminar shear stress also induced c-IAP1 expression. Chase experiments with the use of cycloheximide revealed that 15d-PGJ_2 and shear stress both inhibited the proteolytic degradation of c-IAP1 protein. These results suggested that 15d-PGJ_2 inhibits endothelial cell apoptosis through, at least in part, c-IAP1 protein stabilization. This mechanism might be involved in the antiapoptotic effect of laminar shear stress.

apoptosis; troglitazone; peroxisome proliferator-activated receptor-γ

THE PROSTAGLANDIN (PG) J_2 family, including PGJ_2, Δ^{12}-PGJ_2, and 15-deoxy-$\Delta^{12,14}$-PGJ_2 (15d-PGJ_2), are natural ligands for peroxisome proliferator-activated receptor-γ (PPARγ), a ligand-activated transcription factor nuclear receptor (9, 16). PPARγ ligands, including not only the PGJ_2 family but also the thiazolidinedione class of antidiabetic drugs, modulate several atherogenic processes. They inhibit macrophage activation by inhibiting nitric oxide synthase gene induction (27), the production of inflammatory cytokines (12), and the activation of matrix metalloproteinase-9 (MMP-9) (23). 15d-PGJ_2 also promotes the differentiation of macrophages by stimulating the expression of scavenger receptor CD36 (25, 37). We reported that PGJ_2 and Δ^{12}-PGJ_2 strongly inhibit the proliferation of vascular smooth muscle cells (VSMCs) (30) and that 15d-PGJ_2 induces G_1 arrest and promotes differentiation in VSMCs (24). PPARγ ligands including 15d-PGJ_2 inhibit MMP-9 expression and platelet-derived growth factor-BB-induced migration in VSMCs (22). Moreover, they inhibit the expression of vascular cell adhesion molecule-1 in endothelial cells (11).

Endothelial injury initiates atherogenesis. There are several mechanisms to protect endothelial cells from apoptotic death. One well-known mechanism is shear stress. Laminar fluid shear stress inhibits endothelial cell apoptosis and a lack of shear stress triggers apoptosis (6a). We previously reported that steady laminar shear stress stimulates endothelial cells to express lipocalin-type prostaglandin D synthase (35), which catalyzes the isomerization of PGH_2 to produce PGD_2 (38). PGs of the J_2 family are naturally generated from PGD_2 without specific enzymes (8, 31). In fact, we (35) detected PGD_2 and 15d-PGJ_2 from the culture medium of endothelial cells loaded with shear stress. Therefore, our results suggested that endothelial cells physiologically synthesize the PGJ_2 family. As listed above, most of the effects elicited by the PGJ_2 family seem to be atheroprotective. However, 15d-PGJ_2 has been reported to promote apoptosis in ECV304, which is a so-called endothelial cell-derived cell line, and in human and bovine endothelial cells (3). Therefore, we decided to investigate whether 15d-PGJ_2 really induces apoptosis in normal human endothelial cells with the use of human umbilical vein endothelial cells (HUVECs).

Recently, laminar shear stress has been reported to stimulate the gene expression of a member of the

Address for reprint requests and other correspondence: T. Sasaguri, Dept. of Clinical Pharmacology, Graduate School of Medical Sciences, Kyushu University, 3-1-1 Maidashi, Higashi-ku, Fukuoka, 812-8582, Japan (E-mail: sasaguri@clipharm.med.kyushu-u.ac.jp).

The costs of publication of this article were defrayed in part by the payment of page charges. The article must therefore be hereby marked "*advertisement*" in accordance with 18 U.S.C. Section 1734 solely to indicate this fact.

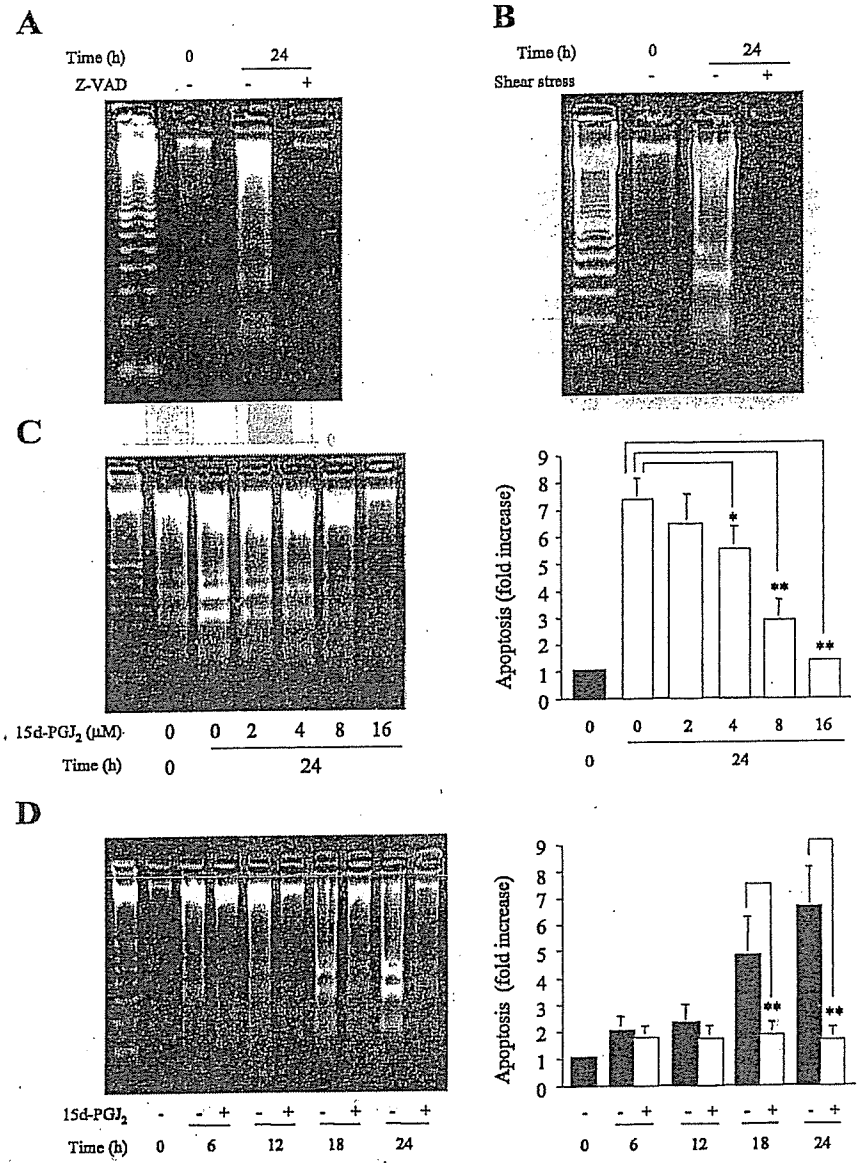

Fig. 1. Shear stress and 15-deoxy-$\Delta^{12,14}$-prostaglandin J_2 (15d-PGJ_2) inhibited DNA ladder formation in human umbilical vein endothelial cells (HUVECs). *A*: HUVECs were cultured in basic fibroblast growth factor (bFGF)-deprived growth medium in the absence or presence of carbobenzoxy-Val-Ala-Asp-CH_2-2,6-dichlorobenzolate (Z-VAD-CH_2-DCB; Z-VAD) (40 μM) for 24 h. Extracted DNA samples were electrophoresed to detect DNA fragmentation. *B*: after exposure to laminar shear stress (15 dyn/cm^2) in bFGF-deprived medium for 24 h, DNA samples were electrophoresed. *C*: HUVECs were incubated in bFGF-deprived medium with various concentrations of 15d-PGJ_2 for 24 h. DNA samples were electrophoresed, and the ladders were quantified with an image analyzer. Values are shown as fold increase (n = 3). $^*P < 0.05$ and $^{**}P < 0.01$. *D*: HUVECs were incubated in bFGF-deprived medium with or without 15d-PGJ_2 (16 μM) for the periods indicated. DNA samples were electrophoresed, and the ladders were quantified. Values are shown as fold increase (n = 3). $^{**}P < 0.01$.

bating them in culture medium deprived of bFGF for 24 h (15). The level of apoptosis was determined by examining oligonucleosomal DNA fragmentation with the use of electrophoresis. bFGF-deprivation markedly increased ladder-like DNA fragmentation (Fig. 1*A*). However, Z-VAD-CH_2-DCB, a caspase inhibitor, completely inhibited the DNA fragmentation, indicating that the fragmentation induced by bFGF deprivation was caused by apoptosis. Instead of Z-VAD-CH_2-DCB, loading laminar shear stress (15 dyn/cm^2) on HUVECs for 24 h also strongly inhibited DNA fragmentation (Fig. 1*B*), indicating that shear stress inhibited endothelial cell apoptosis, consistent with a previous study (14).

15d-PGJ_2 inhibits endothelial cell apoptosis. Because shear stress stimulates endothelial cells to produce 15d-PGJ_2 (35), we investigated the effect of 15d-PGJ_2 on endothelial cell apoptosis. HUVECs were incubated in bFGF-deprived medium with various concentrations of 15d-PGJ_2 for 24 h, and then DNA fragmentation was evaluated by electrophoresis. 15d-PGJ_2 strongly inhibited the DNA fragmentation in a dose-dependent manner with a maximal effect at 16 μM (Fig. 1*C*). Concentrations >32 μM tended to be cytotoxic (not shown). Therefore, we used 16 μM of 15d-PGJ_2 in the following experiments. 15d-PGJ_2 inhibited DNA fragmentation throughout the time course examined (Fig. 1*D*).

Nuclear staining of HUVECs with Hoechst 33258 showed that bFGF deprivation induced a morphological change typical of apoptotic cells, which is nuclear fragmentation with condensed and bright chromatin

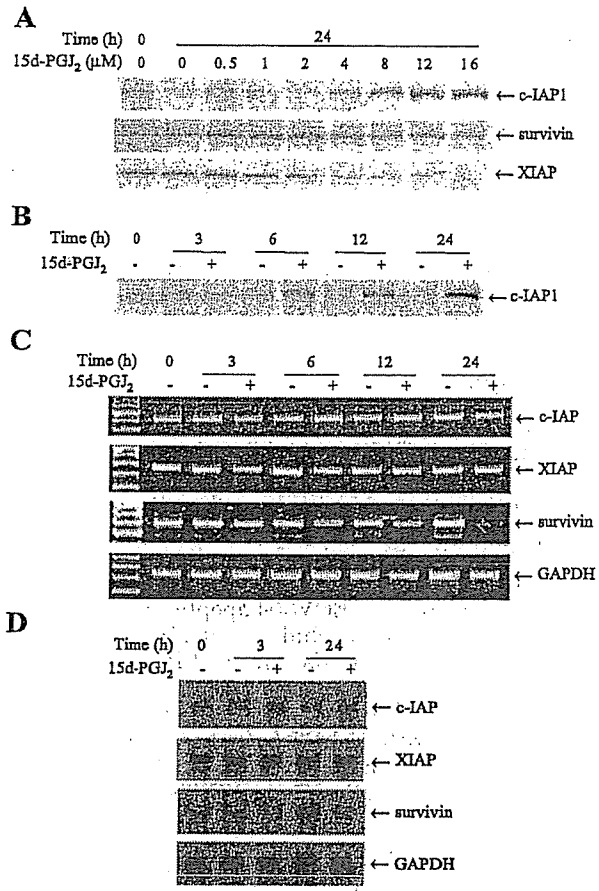

Fig. 3. 15d-PGJ$_2$ induced the cellular inhibitor of apoptosis protein-1 (c-IAP1) expression. *A*: HUVECs were incubated in bFGF-deprived growth medium with various concentrations of 15d-PGJ$_2$ for 24 h and analyzed for the expression of c-IAP1, x-linked IAP (XIAP), and survivin by Western blotting. *B*: HUVECs were incubated in bFGF-deprived medium with 15d-PGJ$_2$ (16 μM) for the periods indicated and were analyzed for c-IAP1 expression by Western blotting. *C*: HUVECs were incubated in bFGF-deprived medium with 15d-PGJ$_2$ (16 μM). Total cellular RNAs extracted at the times indicated were analyzed for the expression of c-IAP1, XIAP, survivin, and GAPDH by RT-PCR. *D*: HUVECs were incubated with 15d-PGJ$_2$ (16 μM) in bFGF-deprived medium. Total cellular RNAs extracted at the times indicated were analyzed for the expressions of c-IAP1, XIAP, survivin, and GAPDH by Northern blotting. One representative result of 3 independent experiments is shown.

tein and incubated the cells with or without 15d-PGJ$_2$ (16 μM) for the periods indicated (Fig. 4, *C* and *D*). Compared with CHX alone, 15d-PGJ$_2$ significantly slowed the rate of degradation of c-IAP1 protein.

Shear stress stabilizes c-IAP1 protein. Recently, Jin et al. (13) reported that laminar shear stress induces the gene expression of c-IAP1 in endothelial cells. In their study, shear stress transiently induced c-IAP1 mRNA with a maximal level being obtained at 4 h. However, they noticed that c-IAP1 protein continued to increase until 24 h, which could not be explained by the transient mRNA expression. Therefore, we examined whether shear stress also stabilizes c-IAP1 protein. Laminar shear stress certainly induced the expression of c-IAP protein, and this was completely inhibited by CHX (Fig. 5*A*). After exposure to shear stress to increase c-IAP1, HUVECs were cultured in the presence of CHX under static conditions or with shear stress (Fig. 5, *B* and *C*). As did 15d-PGJ$_2$, shear stress also

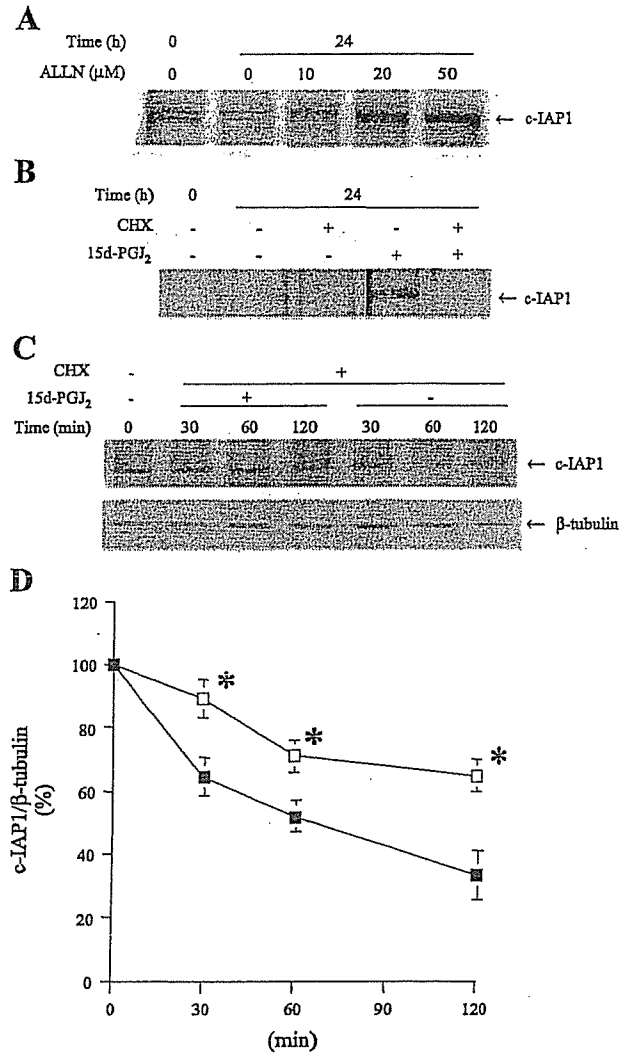

Fig. 4. 15d-PGJ$_2$ inhibited the degradation of c-IAP1 protein. *A*: HUVECs were incubated in bFGF-deprived growth medium with various concentrations of *N*-acetyl-Leu-Leu-norleu-al (ALLN) for 24 h and analyzed for c-IAP1 expression by Western blotting. *B*: HUVECs were incubated in bFGF-deprived medium with or without cycloheximide (CHX; 5 μM) and 15d-PGJ$_2$ (16 μM) for 24 h and were analyzed for c-IAP1 expression by Western blotting. *C*: HUVECs were incubated in bFGF-deprived medium with ALLN (20 μM) for 24 h to induce the expression of c-IAP1 protein. After ALLN was washed out, cells were further incubated with or without 15d-PGJ$_2$ (16 μM) in the presence of CHX (5 μM) for the periods indicated. The expression levels of c-IAP1 protein were analyzed by Western blotting. *D*: data obtained in *B* were quantified. The expression levels of c-IAP1 protein normalized to those of β-tubulin are shown as percentages of the value obtained at *time 0*. $^*P < 0.05$ vs. the values obtained in the absence of 15d-PGJ$_2$ ($n = 4$). □, 15d-PGJ$_2$; ■, control.

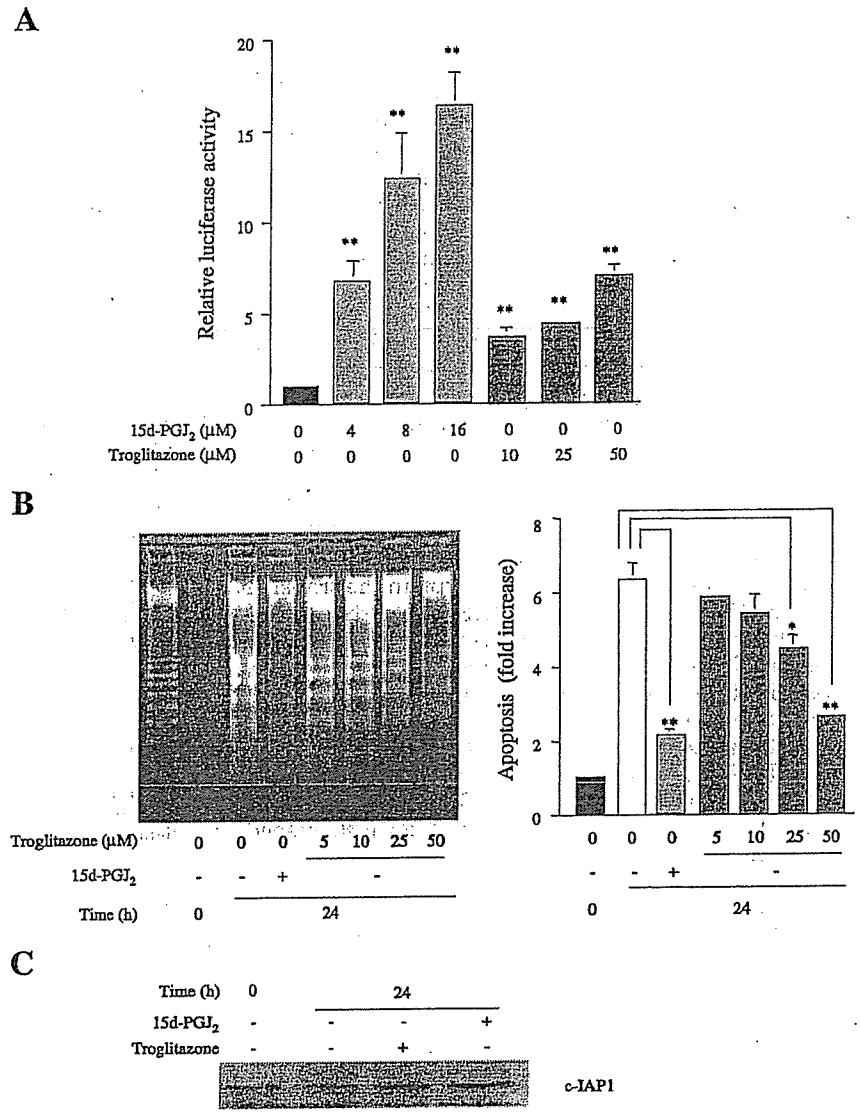

Fig. 6. Effect of troglitazone on HUVEC apoptosis. *A*: after transfection with pCMX-hPPARγ1, tk-PPREx 3-LUC, and pRL-SV40, bovine aortic endothelial cells (BAECs) were stimulated with various concentrations of 15d-PGJ$_2$ or troglitazone for 24 h and were assayed for luciferase activity. The activities normalized to those of *Renilla* luciferase are shown as fold increase against the value obtained in the control cells. $^{**}P < 0.01$ vs. control ($n = 3$). *B*: HUVECs were incubated in bFGF-deprived medium with 15d-PGJ$_2$ (16 μM) or various concentrations of troglitazone for 24 h. Extracted DNA samples were electrophoresed and the ladders were quantified. Values are shown as fold increase against the value obtained at *time 0*. $^{*}P < 0.05$; $^{**}P < 0.01$ ($n = 3$). *C*: HUVECs were incubated with troglitazone (50 μM) or 15d-PGJ$_2$ (16 μM) in bFGF-deprived medium for 24 h and analyzed for c-IAP1 expression by Western blotting.

viral inhibitory repeat (BIR), because the IAP family was originally identified in baculoviruses (6). These proteins regulate programmed cell death in a wide variety of organisms (7). The human IAP family includes c-IAP1, c-IAP2, XIAP, survivin, and neuronal apoptosis inhibitory protein (6). c-IAP1, c-IAP2, and XIAP strongly inhibit the activity of caspases-3, -7, and -9. c-IAP1 and XIAP are degraded by the ubiquitin-proteasome system and inhibition of proteasomes blocks the decrease in IAP expression induced by the apoptotic stimuli (39). In addition to the BIR domain, c-IAP1, c-IAP2, and XIAP contain a zinc-binding really interesting new gene (RING) finger domain at the COOH-terminal end (6). Ubiquitination of protein is dependent on an intact RING finger (20) and c-IAP1 and XIAP catalyze their own ubiquitination in vitro and this reaction requires the RING domain as well (39).

In our study, 15d-PGJ$_2$ upregulated the expression of c-IAP1 protein through stabilization; however, XIAP was not upregulated by 15d-PGJ$_2$ despite the presence of the RING finger domain. The reason for this difference is not clear. 15d-PGJ$_2$ may not stabilize c-IAP1 protein simply via the RING finger domain. As to the mechanism of c-IAP1 stabilization by 15d-PGJ$_2$, a recent report (34) shows that in a leukemia cell line, K562, which lacks tumor suppressor p53, externally introduced p21, a cyclin-dependent kinase inhibitor, inhibited the degradation of c-IAP1. Because p21 is induced by 15d-PGJ$_2$ in VSMCs (24) and was also induced in HUVECs (not shown), c-IAP1 stabilization might be the result of p21 induction.

tosis in human endothelial cells. *Arterioscler Thromb Vasc Biol* 21: 1846–1851, 2001.
20. **Lorick KL, Jensen JP, Fang S, Ong AM, Hatakeyama S, and Weissman AM.** RING fingers mediate ubiquitin-conjugating enzyme (E2)-dependent ubiquitination. *Proc Natl Acad Sci USA* 96: 11364–11369, 1999.
21. **MacLeod RA, Dirks WG, Matsuo Y, Kaufmann M, Milch H, and Drexler HG.** Widespread intraspecies cross-contamination of human tumor cell lines arising at source. *Int J Cancer* 83: 555–563, 1999.
22. **Marx N, Schönbeck U, Lazar MA, Libby P, and Plutzky J.** Peroxisome proliferator-activated receptor gamma activators inhibit gene expression and migration in human vascular smooth muscle cells. *Circ Res* 83: 1097–1103, 1998.
23. **Marx N, Sukhova G, Murphy C, Libby P, and Plutzky J.** Macrophages in human atheroma contain PPARγ: differentiation-dependent peroxisomal proliferator-activated receptor γ (PPARγ) expression and reduction of MMP-9 activity through PPARγ activation in mononuclear phagocytes in vitro. *Am J Pathol* 153: 17–23, 1998.
24. **Miwa Y, Sasaguri T, Inoue H, Taba Y, Ishida A, and Abumiya T.** 15-Deoxy-$\Delta^{12,14}$-prostaglandin J_2 induces G_1 arrest and differentiation marker expression in vascular smooth muscle cells. *Mol Pharmacol* 58: 837–844, 2000.
25. **Nagy L, Tontonoz P, Alvarez JG, Chen H, and Evans RM.** Oxidized LDL regulates macrophage gene expression through ligand activation of PPARγ. *Cell* 93: 229–240, 1998.
26. **Padilla J, Kaur K, Cao HJ, Smith TJ, and Phipps RP.** Peroxisome proliferator activator receptor-γ agonists and 15-deoxy-$\Delta^{12,14}$-PGJ_2 induce apoptosis in normal and malignant B-lineage cells. *J Immunol* 165: 6941–6948, 2000.
27. **Ricote M, Li AC, Willson TM, Kelly CJ, and Glass CK.** The peroxisome proliferator-activated receptor-γ is a negative regulator of macrophage activation. *Nature* 391: 79–82, 1998.
28. **Rohn TT, Wong SM, Cotman CW, and Cribbs DH.** 15-Deoxy-$\Delta^{12,14}$-prostaglandin J_2, a specific ligand for peroxisome proliferator-activated receptor-γ, induces neuronal apoptosis. *Neuroreport* 12: 839–843, 2001.
29. **Rossi A, Kapahi P, Natoli G, Takahashi T, Chen Y, Karin M, and Santoro MG.** Anti-inflammatory cyclopentenone prostaglandins are direct inhibitors of IκB kinase. *Nature* 403: 103–108, 2000.
30. **Sasaguri T, Masuda J, Shimokado K, Yokota T, Kosaka C, Fujishima M, and Ogata J.** Prostaglandins A and J arrest the cell cycle of cultured vascular smooth muscle cells without suppression of *c-myc* expression. *Exp Cell Res* 200: 351–357, 1992.
31. **Shibata T, Kondo M, Osawa T, Shibata N, Kobayashi M, and Uchida K.** 15-Deoxy-$\Delta^{12,14}$-prostaglandin J_2: a prostaglandin D_2 metabolite generated during inflammatory processes. *J Biol Chem* 277: 10459–10466, 2002.
32. **Shimada T, Kojima K, Yoshiura K, Hiraishi H, and Terano A.** Characteristics of the peroxisome proliferator activated receptor γ (PPARγ) ligand induced apoptosis in colon cancer cells. *Gut* 50: 658–664, 2002.
33. **Suzuki A, Hayashida M, Ito T, Kawano H, Nakano T, Miura M, Akahane K, and Shiraki K.** Survivin initiates cell cycle entry by the competitive interaction with Cdk4/p16^{INK4a} and Cdk2/cyclin E complex activation. *Oncogene* 19: 3225–3234, 2000.
34. **Suzuki A, Tsutomi Y, Akahane K, Araki T, and Miura M.** Resistance to Fas-mediated apoptosis: activation of caspase 3 is regulated by cell cycle regulator p21^{WAF1} and IAP gene family ILP. *Oncogene* 17: 931–939, 1998.
35. **Taba Y, Sasaguri T, Miyagi M, Abumiya T, Miwa Y, Ikeda T, and Mitsumata M.** Fluid shear stress induces lipocalin-type prostaglandin D_2 synthase expression in vascular endothelial cells. *Circ Res* 86: 967–973, 2000.
36. **Takahashi K, Sawasaki Y, Hata J, Mukai K, and Goto T.** Spontaneous transformation and immortalization of human endothelial cells. In vitro *Cell Dev Biol* 26: 265–274, 1990.
37. **Tontonoz P, Nagy L, Alvarez JG, Thomazy VA, and Evans RM.** PPARγ promotes monocyte/macrophage differentiation and uptake of oxidized LDL. *Cell* 93: 241–252, 1998.
38. **Urade Y and Hayaishi O.** Prostaglandin D synthase: structure and function. *Vitam Horm* 58: 89–120, 2000.
39. **Yang Y, Fang S, Jensen JP, Weissman AM, and Ashwell JD.** Ubiquitin protein ligase activity of IAPs and their degradation in proteasomes in response to apoptotic stimuli. *Science* 288: 874–877, 2000.